scientific reports



OPEN

Automated vacuum drying kinetics, thermodynamics, and economic analysis of sage leaves

Nabil Eldesokey Mansour¹, Khaled A. Metwally², Aml Abubakr Tantawy³, Ahmed Elbeltagi⁴, Ali Salem^{5,6}, Ahmed Z. Dewidar^{7,8}, Abdelaziz M. Okasha⁹, Moustapha Eid Moustapha¹⁰ & Abdallah Elshawadfy Elwakeel¹¹

Vacuum drying of sage leaves is important for preserving their essential oils, flavor, and medicinal properties by reducing oxidation and thermal degradation, but previous research has not investigated its impact on drying speed, thermodynamic properties, mathematical modeling, or economic viability. This study employed an automatic vacuum dryer at temperatures of 40 °C, 50 °C, and 60 °C under different pressure conditions (atmospheric, -5 kPa, and -10 kPa) with a 1 cm layer thickness. Results showed that increasing temperature and decreasing pressure significantly improved drying efficiency, reducing the process time to just 90 min while achieving a drying rate of 22.34 kg water/ kq dry matter/h and an effective moisture diffusivity of 6.716 × 10⁻⁹ m²/s under optimal conditions (60 °C and -10 kPa). The Page model was identified as the most suitable for describing the thin-layer drying behavior. Thermodynamic analysis revealed activation energy values between 19.4 and 37.7 kJ/ mol, with activation enthalpy decreasing at higher temperatures and lower pressures. The negative activation entropy values indicated chemical adsorption or structural modifications during drying. From an economic perspective, the most efficient drying conditions reduced the payback period to less than two months, demonstrating strong commercial potential. These findings highlight the industrial promise of vacuum drying for herb processing, with future research opportunities in process optimization, application to other herbs, and sustainability assessments to further enhance efficiency and economic benefits.

Keywords Activation entropy, Free energy of Gibbs, Internet of things (IoT), Medicinal and aromatic plants, Thin layer modeling

Sage (Salvia officinalis L.), a versatile and aromatic herb, is globally valued for its culinary, medicinal, and ornamental uses^{1,2}. Originating from the Mediterranean region³, sage is renowned for its distinctive flavor and health benefits, including anti-inflammatory, antioxidant, and antimicrobial properties. Its essential oils and bioactive compounds, such as thujone and rosmarinic acid, make it a key ingredient in herbal remedies, cosmetics, and natural health products^{4–6}. Globally, sage is cultivated in temperate climates with well-drained soils, with major producers including countries in Europe, North America, and the Middle East^{7,8}.

Sage production is gaining importance in Libya due to the country's favorable climate and agricultural expertise. Where grown primarily in regions with adequate sunlight and irrigation, sage is prized for its high quality and potency. Local farmers cultivate sage for both domestic use and export, contributing to the country's

¹Agricultural Engineering Department, Faculty of Agriculture, Damanhour University, Damanhour, Egypt. ²Soil and Water Sciences Department, Faculty of Technology and Development, Zagazig University, Zagazig 44519, Egypt. ³Food Science Department, Faculty of Agriculture, Beni-Suef University, Beni-Suef 65211, Egypt. ⁴Agricultural Engineering Department, Faculty of Agriculture, Mansoura University, Mansoura 35516, Egypt. ⁵Civil Engineering Department, Faculty of Engineering, Minia University, Minia 61111, Egypt. ⁶Structural Diagnostics and Analysis Research Group, Faculty of Engineering and Information Technology, University of Pécs, Pécs 7622, Hungary. ⁷Prince Sultan Bin Abdulaziz International Prize for Water Chair, Prince Sultan Institute for Environmental, Water and Desert Research, King Saud University, Riyadh 11451, Saudi Arabia. ⁸Department of Agricultural Engineering, College of Food and Agriculture Sciences, King Saud University, Riyadh 11451, Saudi Arabia. ⁹Department of Agricultural Engineering, Faculty of Agriculture, Kafrelsheikh University, Kafr El-Sheikh 33516, Egypt. ¹⁰Department of Chemistry, College of Science and Humanities, Prince Sattam bin Abdulaziz University, Al-Kharj 11942, Saudi Arabia. ¹¹Agricultural Engineering Department, Faculty of Agriculture and Natural Resources, Aswan University, Aswan 81528, Egypt. ¹²Eemail: khametwally@zu.edu.eg; salem.ali@mik.pte.hu; adewidar@ksu.edu.sa

agricultural economy. The herb is processed into dried leaves, teas, and essential oils, catering to both local markets and international demand. Libya's sage production not only supports sustainable farming practices but also highlights the country's potential as a key player in the global herbal industry^{7,9–11}.

Drying is an essential process for preserving the quality, flavor, and medicinal properties of sage, but traditional drying methods often fall short in maintaining the herb's integrity^{12–14}. Industrial dryers, while efficient and capable of handling large volumes, typically operate at high temperatures, which can degrade heat-sensitive bioactive compounds such as essential oils, flavonoids, and phenolic acids. This thermal degradation not only diminishes sage's aromatic and therapeutic qualities but also reduces its market value^{15,16,13}. Additionally, industrial dryers are energy-intensive, contributing to higher production costs and environmental impact^{17–19}. Furthermore, open sun drying, a widely used method due to its low cost and simplicity, presents its own set of challenges^{20–22}. This method is highly dependent on weather conditions, making it inconsistent and time-consuming^{23,24}. Moreover, sage dried in open sunlight is exposed to contamination from dust, insects, and microorganisms, which can compromise its safety and quality^{25–27}. Prolonged exposure to UV radiation and fluctuating temperatures can also lead to the loss of volatile compounds and discoloration, further reducing the herb's appeal^{28,29}.

In contrast, vacuum drying has emerged as a superior alternative, addressing the limitations of traditional methods. By operating at low temperatures and in an oxygen-free environment, vacuum drying minimizes thermal degradation and oxidation, preserving sage's essential oils, vibrant color, and bioactive compounds^{30–32}. This method ensures a higher-quality product with enhanced shelf life, making it ideal for culinary, medicinal, and cosmetic applications^{33,34}. Furthermore, vacuum drying is energy-efficient and scalable, offering a sustainable solution for modern herb processing. Its ability to maintain the functional and sensory properties of sage underscores its importance in the post-harvest industry, paving the way for improved product quality and economic value^{35,36}.

Many previous studies were conducted on drying of sage leaves including, Venskutonis³⁷ studied the effect of drying on the volatile constituents; Sellami et al.³⁸ studied the effect of drying on chemical composition, and radical scavenging activity of the essential oil; Sadowska et al.³⁹ evaluated effects of drying method of the concentration of compounds on sage; Esturk⁴⁰ investigated the effect of intermittent and continuous microwaveconvective air-drying characteristics of sage leaves; Hamrouni-Sellami et al.⁴¹ determined the effects of seven drying methods on total phenolics, flavonoids, individual phenolics, and antioxidant activity of the methanol extract of sage; Hassanain⁴² used different types of passive solar dryer for drying sage; Esturk et al.⁴³ dried sage inflorescences by intermittent and continuous microwave-convective air combination; Belghit et al. 44 experimentally studied the drying kinetics of sage in a drying tunnel working in forced convection; Doymaz et al.⁴⁵ studied the effect of air temperature on drying kinetics, color changes and total phenolic content of sage leaves; Salehi et al. 46 studied the effect of drying methods on rheological and textural properties, and color changes of wild sage seed gum; Şahin-Nadeem et al.⁴⁷ experimentally studied the influence of inlet air temperature and carrier material on the production of instant soluble sage by spray drying; Baltacı et al. 48 studied the effects of spray and freeze-drying methods on aroma compounds, sensory characteristics, physicochemical composition, antioxidant and antimicrobial properties of instant sage tea; and Amini et al.⁴⁹ studied the effect of infrared drying on drying kinetics and color changes of wild sage seed mucilage. To date, there has been a lack of research investigating the impact of evacuated drying on sage leaves with respect to drying kinetics, thermodynamic properties, mathematical modeling, and the economic analysis of the drying process. This absence of investigation highlights a significant gap in the existing literature, emphasizing the necessity for comprehensive studies that thoroughly explore these variables. A deeper understanding of the relationship between drying methods and their economic consequences could facilitate the development of more efficient and sustainable practices within various agricultural sectors.

This research paper aims to investigate the drying kinetics of sage leaves, focusing on various parameters, including accumulated weight loss, moisture content, moisture ratio, drying rate, EMD, and activation energy. The study will also address mathematical modeling, thermodynamic properties, and economic analysis of a developed automatic vacuum dryer (DAVD) designed for sage leaves. The objective of this research is to provide critical data that will aid in identifying the optimal drying model to enhance the commercial drying process of sage leaves. The findings of this study will be of particular significance to professionals in postharvest technology who are seeking to improve the efficiency of their drying methods. Moreover, the results may assist in the formulation of industry standards that promote consistent quality in the final product. By optimizing the drying process, producers can increase their yields and enhance the marketability of sage leaves.

Materials and methods Experimental setup

During the current study, sage plants were harvested from a local farm in Al-Faydiyah, Al-Jabal Al-Akhdar, Libya, and stored in a refrigerator at 4 °C before use. All drying experiments were conducted in the laboratory of the Department of Agricultural Engineering, Faculty of Agriculture, Omar Al-Mukhtar University, Libya, after the plucking season of 2021. The plants were washed with tap water to remove dirt and dust. Then they were gently watered and wiggled to dry from the water. Excess water was then wiped off with paper towels. The initial moisture content was then determined by the hot air furnace method using a laboratory furnace. An electronic balance was used to weigh the samples, with each sample weighing 100 g. The experiment was conducted in triplicate, and the average was taken. The initial moisture content before drying was 85.5%. All drying experiments were conducted with a layer thickness of 1 cm. Additionally, the sage leaf samples were dried at three operating pressures (P1 = normal atmospheric pressure (atm), P2 = -5 kPa, and P3 = -10 kPa) and three drying temperatures (T1 = 40, T2 = 50, and T3 = 60 °C). All drying experiments were conducted until constant weight and reaching the equilibrium moisture content. The moisture content during the drying process



Fig. 1. Main components of the DAVD. Whereas (1) Laptop, (2) Arduino uno board, (3) Control unit, (4) Vacuum pump, and (5) Vacuum gauge.

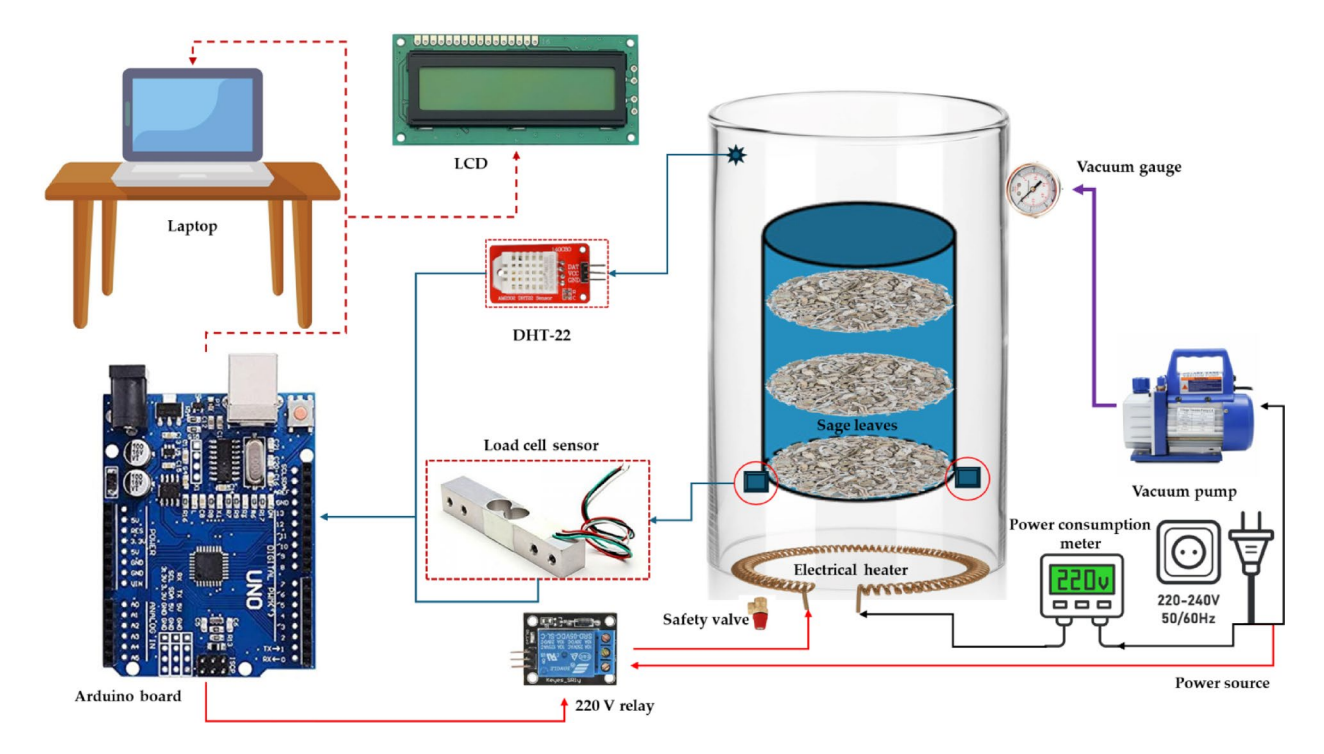


Fig. 2. Schematic view showing different components of the DAVD.

was estimated by weighing the samples periodically with load sensors every 15 min. Furthermore, the relative humidity and temperature of the air inside the dryer were measured with the developed measuring unit.

Description of the DAVD

As shown in Figs. 1 and 2, the DAVD was manufactured using available materials in local markets in Libya. The DAVD consists of many parts, such as (1) Main body: it was manufactured from reused iron sheets with an average capacity of 200 L; (2) Vacuum pump: A half-hp vacuum pump (model: Vp245, China) regulates the pressure inside the dryer. It can control pressure in a range from -1 to 3 bars. It is crucial for DAVD as they

create and maintain a low-pressure environment, enabling efficient moisture removal at lower temperatures. This preserves heat-sensitive materials, reduces energy consumption, and speeds up drying processes; (3) Vacuum gauge: This instrument measures the pressure inside the dryer and regulates its level. It can measure the pressure in a range from -0.1 to 6.0 MPa with an accuracy of ± 0.5 ; (4) Electrical heater: It was used for increasing the air temperature inside the DAVD based on the requirements of the drying process; it has a rated power of 600 watts and is installed in the bottom of the dryer; (5) Load cell sensor: A pair of load cell sensors was used to automatically measure the weight of the sage leaf samples and send the signals to an Arduino board; (6) Relative humidity and temperature sensor: It was used to accurately measure the relative humidity and temperature inside the DAVD; (7) Relay: it was used for controlling the operation of the electrical heater automatically based on the output signals from the DHT-22 and the Arduino Uno board; (8) Control unit: it consists of an Arduino board (model: Arduino Uno, China). It is a microcontroller board based on the ATmega328P. It has 14 digital input/output pins (of which 6 can be used as PWM outputs), 6 analog inputs, a 16 MHz ceramic resonator, a USB connection, a power jack, an ICSP header, and a reset button; (9) Terminal device: The DAVD is integrated with an LCD to present the temperature and humidity signals directly for the user, but during the laboratory experiments, the output signals were transmitted to a laptop and stored in an Excel sheet for subsequent analysis.

Evaluations processes of the DAVD

Drying kinetics

Moisture content (μ_d) The initial moisture content of sage leaves in a laboratory is estimated by following the approach defined by AOAC⁵⁰, utilizing the oven-drying method. And it was calculated according to Eq. 1^{51,52}.

$$\mu_d = \left[\frac{W_w - W_d}{W_d}\right] \times 100 \tag{1}$$

where, W_w and W_d is the wet and dry weight of henna leaf sample, respectively in g.

Accumulated weight loss of assess weight loss during the desiccation of sage leaves, the subsequent procedures are implemented: The fresh sage leaves (W_t) are measured using a precision electronic balance with an accuracy of ± 0.1 g. The fresh sage leaves are thereafter distributed uniformly on the drying trays and positioned in the DAVD. Every 15 min, the weight of the sage leaves sample was recorded using the load cell sensor, and the observed weight (W_{t+1}) was documented in an Excel spreadsheet on the laptop. Drying persists until the weight stabilizes (constant weight, W_3). Weight loss is determined using Eq. $2^{53,54}$.

$$Weight loss (g) = W_t - W_{t+1}$$
 (2)

<u>Drying rate</u> The evaluation of drying rates is essential in sectors such as food, pharmaceuticals, and agriculture, as it assesses the time and energy needed to eliminate moisture from substances. It entails the examination of variables such as temperature, humidity, airflow, and material characteristics. Precise estimation guarantees effective drying, maintains product quality, and maximizes energy efficiency in industrial processes. The drying rate was determined using Eq. 3⁵⁵.

Drying rate
$$(g_{water}/g_{dry\ matter}.h) = \frac{Weight \ loss\ (g)}{\Delta t\ (h)}$$
 (3)

Moisture ratio (MR) The moisture ratio calculation is a critical metric in drying processes, indicating the proportion of residual moisture content (M_t) in a material relative to its original moisture content (M_0). Monitoring drying efficiency, estimating drying durations, and guaranteeing product quality are crucial. Through the analysis of moisture ratio, sectors such as food, agriculture, and pharmaceuticals can enhance drying conditions, minimize energy usage, and avert both over-drying and under-drying. Precise computation aids in sustaining uniformity, extending shelf life, and augmenting total process efficiency^{23,24,52,56,57}. The moisture ratio of the dried sage leaf samples was determined using Eq. 4^{58} .

$$MR = \frac{M_t - M_e}{M_0 - M_e} \tag{4}$$

The moisture ratio was utilized to analyze the drying kinetics of sage leaves by appropriate mathematical models. The value of equilibrium moisture content (M_e) can be disregarded, as it is rather little relative to the values of M_t and M_0 . Therefore, the moisture ratio can be represented as shown in Eq. 5⁵⁹.

$$MR = \frac{M_t}{M_0} \tag{5}$$

Drying constant (k)

The drying constant (k) in thin-layer drying is derived from a mixture of many drying transport variables, including mass coefficients, density, specific heat, thermal conductivity, and interfacial heat transfer. The drying constant is determined through the exponential relationship between LnMR and drying time. Furthermore, the drying constant is derived from the same relationship for the DAVD across three operating pressures and three drying temperatures of the sage leaves. While drying constants are crucial for comprehensively defining the

drying kinetics of dried product^{60,61}, it is vital to consider the diverse transport parameters involved. The drying constant was determined utilizing Eq. 6.

$$MR = A \exp(-k \times t) \tag{6}$$

Effective moisture diffusivity (EMD)

Fick's second law of diffusion is an effective framework for comprehending and forecasting moisture diffusion dynamics in materials. Utilizing this idea, researchers and engineers can acquire significant insights into EMD, facilitating progress in several domains dependent on moisture transport regulation⁶². The general equation for mass transfer in a slab shape is shown in Eq. 7^{63,64}:

$$\frac{\partial M}{\partial t} = D_{eff} \left(\frac{\partial^2 M}{\partial r^2} + \frac{2}{r} \frac{\partial M}{\partial r} \right) \tag{7}$$

$$M(r,t)|_{t=0} = M_0 (8)$$

$$\left. \frac{\partial M(r,t)}{\partial r} \right|_{t=0} = 0 \tag{9}$$

$$M\left(R,t\right)|_{t>0} = M_e \tag{10}$$

With the appropriate initial and boundary conditions:

where: M is the moisture content, % (w.b.) and t is the drying time, s.

The initial boundary condition specifies that moisture is uniformly distributed across the sage leaf sample. The second indicates that the mass transfer is symmetrical relative to the center of the sage leaf sample. The third criterion stipulates that the surface moisture content of the sage leaf sample rapidly attains equilibrium with the ambient air conditions. The values of equilibrium moisture content (*Me*) are rather minimal. Consequently, the third condition can be condensed into Eq. 11.

$$M(R,t)|_{t>0} = 0$$
 (11)

Following the numerical procedure, assume a solution of the following form to separate the variables:

$$M(r,t) = F(r) *G(t)$$
(12)

where F is function of r only, and G is function of t only.

$$\frac{M_0 - M}{M_0} = 1 - \frac{8}{\pi^2} \sum_{n=0}^{\infty} \left(\frac{1}{n^2} exp\left(\frac{-\pi^2 \times D_{\text{eff}} \times t}{4L^2} \right) \right)$$
 (13)

Equation 14 was generated by simplify Eq. 13:

$$\frac{M}{M_0} = \frac{8}{\pi^2} \sum_{n=0}^{\infty} \left(\frac{1}{n^2} exp\left(\frac{-\pi^2 \times D_{\text{eff}} \times t}{4L^2}\right) \right)$$
 (14)

Based on the previous moisture ratio (MR) equation and the third boundary condition, Eq. 15 was simplified as follows:

$$MR = \frac{8}{\pi^2} \times \sum_{n=1}^{\infty} \frac{1}{n^2} \exp\left(\frac{-\pi^2 \times D_{eff} \times t}{4L^2}\right)$$
 (15)

The diffusion coefficients are typically determined by plotting experimental drying data in terms of ln (MR) versus drying time (t), because the plot gives a straight line with a slope as $\left[\pi^2 \frac{D_{eff}}{R^2}\right]^{65-69}$:

$$MR = \frac{8}{\pi^2} \times A \exp\left(\frac{-\pi^2 \times D_{\text{eff}} \times t}{4L^2}\right)$$
 (16)

Also, Eq. 17 has been obtained mathematically from Eq. 16,

$$\ln (MR) = \ln \left(\frac{8}{\pi^2}\right) - \left(\frac{\pi^2 \times D_{\text{eff}} \times t}{4L^2}\right)$$
(17)

Activation energy

The activation energy (E_a) for the process was determined by applying the Arrhenius equation, following an analogous methodology to that used for calculating the effective diffusion coefficient ($D_{\rm eff}$). This approach establishes the temperature dependence of both parameters, where the natural logarithm of each was plotted

against the reciprocal of absolute temperature (1/T). The resulting linear relationships enabled the calculation of E_a from the slope of ln(k) versus 1/T, while $D_{\rm eff}$ was similarly derived from its temperature-dependent behavior, demonstrating consistent thermodynamic treatment of both kinetic parameters⁷⁰.

$$D_{\text{eff}} = D_0 \exp\left(-\frac{E_a}{RT}\right) \tag{18}$$

where, D_0 is the pre-exponential factor (frequency factor, s⁻¹), R is the universal gas constant (8.314 J/mol.K), and T is the absolute temperature in K.

Mathematical modeling of drying process

The experimental data obtained from drying sage leaves at different drying temperatures and operating pressures were evaluated using nine mathematical models (Table 1). Subsequently, non-linear regression analysis was performed using the developed model by Öksüz and Buzrul⁷¹, to estimate the coefficients of the specified models and statistical metrics (root mean squared error (RMSE), coefficient of determination (R^2 and adjusted coefficient of determination (R^2 and maximal R^2 and R^2 and

$$R^{2} = 1 - \frac{\sum (MR_{experimental} - MR_{fitted})^{2}}{\sum (MR_{experimental} - MR_{mean})^{2}}$$
(19)

$$R_{adj.}^2 = 1 - \left(1 - R^2\right) * \frac{n-1}{n-p} \tag{20}$$

where $MR_{experimental}$ and MR_{fitted} are the observed (experimental) value and fitted value by the model, respectively and MR_{mean} is the average value of the experimental data in Eq. 19, n is the number of data points and p is the number of parameters in the model⁷¹. RMSE value is calculated as follows⁷¹:

$$RMSE = \sqrt{\frac{\sum (MR_{experimental} - MR_{fitted})^2}{n - p}}$$
 (21)

Note that the term in the numerator of Eq. 19 or Eq. 21 is the sum of squared error (SSE) and the term in the denominator of Eq. 19 is sum of squared total (SST). Regretfully, the denominator of RMSE calculation in certain thin-layer modeling literature only includes n; however, it should be n-p because degrees of freedom is the difference between the experimental data and the model, that is, error.

Thermodynamic parameters

Thermodynamic parameters, activation enthalpy (ΔH^{\ddagger}) in J/K.mol and activation entropy (ΔS^{\ddagger}) in J/K.mol, were estimated using Eq. 22^{81,82}.

$$\ln\left(\frac{k}{T}\right) = \left\lceil \left(\frac{\ln k_B}{h}\right) + \left(\frac{\Delta S^{\ddagger}}{R}\right) - \left(\left(\frac{\Delta H^{\ddagger}}{R}\right) \times \left(\frac{1}{T}\right)\right) \right\rceil$$
 (22)

where k_B is Boltzmann's constant (1.38065×10⁻²³ J/K), h the Planck constant (6.62608×10⁻³⁴ J.s), and the notation ‡ refers to the state of activated complex.

No.	Model name	Model equation*	Reference
1	Aghbashlo	$MR = \exp\left(-\frac{k_1 t}{1 + k_2 t}\right)$	71,75
2	Logarithmic (Asymptotic)	MR = a*exp(-kt) + c	76-78
3	Midilli	$MR = a^* \exp(-kt^n) + bt$	
4	Modified midilli I	$MR = \exp\left(-kt^n\right) + bt$	79,80
5	Modified midilli II	$MR = a^* \exp(-kt^n) + b$	79
6	Page	$MR = \exp\left(-kt^n\right)$	76-78
7	Wang-Sigh	$MR = 1 + bt + at^2$	
8	Weibullian	$MR = \exp\left(-\left(\frac{t}{\alpha}\right)^{\beta}\right)$	79,80
9	Weibullian I	$MR = 10^{-\left(\frac{t}{\delta}\right)^n}$	

Table 1. List of mathematical models used during the current study. * MR is the moisture ratio, dimensionless: t is the drying time, min: k_1 , k_2 and k are the drying constants, min⁻¹: a, b, c, n, γ , β and δ are the models constants, dimensionless: RMSE is the root mean square error: R^2 is the coefficient of determination R^2_{adj} . is the adjusted coefficient of determination. All statistical analysis was conducted at $p \le 0.05$.

According to Eq. 22, the regression of ln k/T versus 1/T (K⁻¹), gives a straight line with the slope $\left(\frac{\Delta H^{\ddagger}}{R}\right)$ and the interception $\left[\left(\frac{\ln k_B}{h}\right) + \left(\frac{\Delta S^{\ddagger}}{R}\right)\right]$, which allows the determination of ΔH^{\ddagger} and ΔS^{\ddagger} , respectively. While the Gibbs free energy of activation (ΔG^{\ddagger}) was determined for each temperature using Eq. 23⁸².

$$\Delta G^{\dagger} = \Delta H^{\dagger} - T \Delta S^{\dagger} \tag{23}$$

Economic analysis

An economic examination of the drying process and dryers is essential for increasing efficiency, minimizing costs, and improving sustainability. Drying is energy-intensive and frequently constitutes a substantial amount of operational costs in sectors such as agriculture, food processing, and manufacturing. By assessing variables like as energy usage, drying duration, equipment expenses, and maintenance, enterprises may pinpoint economical alternatives and enhance profitability. Furthermore, economic analysis aids in the selection of appropriate dryer technology, optimizing capital expenditure against operational savings. It additionally advances environmental objectives by endorsing energy-efficient methods, decreasing waste, and mitigating carbon footprints. This research ultimately secures a competitive advantage by aligning economic and operational performance with market demands^{83–86}. The economic analysis of the DAVD was assessed utilizing Eqs. 24–35. Table 2 presents the calculation assumptions for the economic analysis of the DAVD based on economic aspects in Libya.

The annual investment cost of the DAVD is calculated by summing the capital cost (amortized over its lifespan), annual maintenance expenses, energy consumption costs, and other operational expenditures. This calculation helps determine the annual investment cost, aiding in budgeting, cost optimization, and decision-making for efficient and economical dryer selection and operation. The annual investment cost (C_a in USD/year) of the DAVD was calculated using Eq. 24.

$$C_a = C_{ac} + C_m - V_a \tag{24}$$

The annual capital cost of the DAVD is calculated by dividing the initial purchase cost by its expected lifespan in years, often incorporating interest or financing rates. Where the annual capital cost (C_{ac}) of the DAVD was calculated according to Eqs. 25 and 26, as follows,

$$C_{ac} = C_{cc} \times F_c \tag{25}$$

$$F_c = \frac{d(1+d)^{\tau}}{(1+d)^{\tau} - 1} \tag{26}$$

where C_{cc} is the capital cost of the DAVD, F_c is the recovery factor.

The drying cost per kg of sage leaves using the DAVD (C_s), was calculated using Eq. $27^{87,88}$.

$$C_s = \frac{C_a}{M_y} \tag{27}$$

The amount of dried sage leaves using the DAVD per year (M_y) is calculated using Eq. 28, where the total amount of sage leaves using the DAVD per batch (M_d) was 2 kg. Additionally, the number of days available for drying per year (D_d) assumed to be 350 days.

$$M_y = \frac{M_d \times D}{D_d} \tag{28}$$

Based on local markets in Libya, the cost of fresh sage leaves (C_{fd}) was about 2.0 USD per kg. And the cost of one kilogram of the dried sage leaves (C_{ds}) was calculated using Eq. 29^{87,88}.

$$C_{ds} = C_{dp} + C_s \tag{29}$$

where C_{dp} is the cost of fresh sage leaves per kg of dried product, which is calculated using Eq. 30,

$$C_{dp} = C_{fd} \times \frac{M_f}{M_d} \tag{30}$$

Parameter	Nomenclature	Unit	Value
Interest rate	d	%	3%
Maintenance cost	C_m	USD/year	3% of the annual capital cost
Salvage value	V_a	%	8% of the annual capital cost
Operating life	τ	year	20 years
Inflation rate	i	%	2.5%

Table 2. Calculation assumptions of economic analysis of the DAVD.

where, M_f is the quantity of fresh sage leaves loaded inside the DAVD.

Based on local markets in Libya, the selling price of dried sage leaves (SP_c) is about 5.0 USD per kg. Also, the savings obtained per kg of dried sage leaves (S_{kg}) are given by Eq. 31,

$$S_{kq} = SP_c - C_{ds} \tag{31}$$

The savings obtained from the DAVD per batch (S_b) are given by Eq. 32,

$$S_b = S_{kg} \times M_d \tag{32}$$

While the savings obtained from the DAVD per day (S_d) are given by Eq. 33,

$$S_d = \frac{S_b}{D} \tag{33}$$

The savings obtained from the DAVD after "j" number of years is given by Eq. 34,

$$S_j = S_d \times D \times (1+j)^{j-1} \tag{34}$$

The payback time (T) for the DAVD is calculated using Eq. 35^{87,88}.

$$T = \frac{\ln\left[1 - \frac{C_{cc}}{S_1}(d - i)\right]}{\ln\left(\frac{1+i}{1+d}\right)}$$
(35)

where, S_1 is the savings obtained from the DAVD after the first year.

Results and discussions

Accumulated weight loss and moisture content

Many crops experience significant weight loss, adversely affecting their quality and reducing profitability. For instance, they may deteriorate in shape or texture, or the color may become compromised. The principal factor contributing to weight loss is the leaching and diffusion process, wherein water-soluble constituents such as vitamins, flavors, minerals, carbs, sugars, and proteins are extricated from plant tissue into the environment. Figure 3 illustrates the cumulative weight losses of sage leaves under varying operating pressures and drying temperatures. The depicted data in the figure indicated that the weight loss of sage leaves remained consistent across various treatments. However, weight loss escalated with rising drying temperatures and operating pressures. The maximum weight loss occurred at an air temperature of 60 °C and an operating pressure of –10 kPa (about 14.6 g), whereas the minimum weight loss was recorded at an air temperature of 40 °C and atmospheric pressure (about 14.4 g). This suggests that weight loss correlates positively with increased power; higher power results in greater weight loss. Kidmose et al. and Wang et al. encountered a similar phenomenon. Additionally, Fig. 3 demonstrated that considerable moisture loss occurred during the declining rate period, supporting results from various prior studies 2-94. Moreover, samples of dried sage leaves attained an equilibrium moisture content ranging from 13.1 to 13.7% (wet basis).

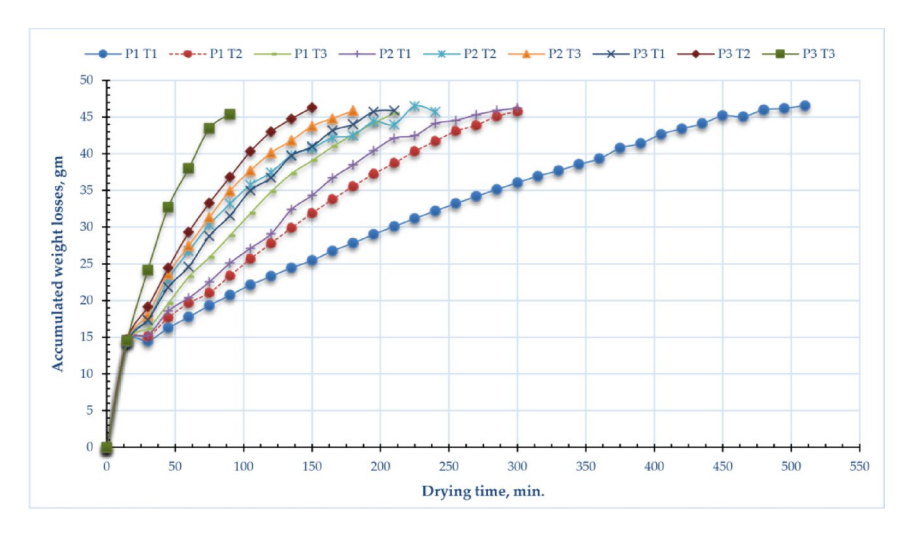


Fig. 3. Accumulated weight losses of sage leaves for DAVD at different levels of drying pressures (P1 = atm; P2 = -5 kPa and P3 = -10 kPa) and drying temperatures (T1 = 40, T2 = 50 and T3 = $60 \, ^{\circ}$ C)^{53,95-97}.

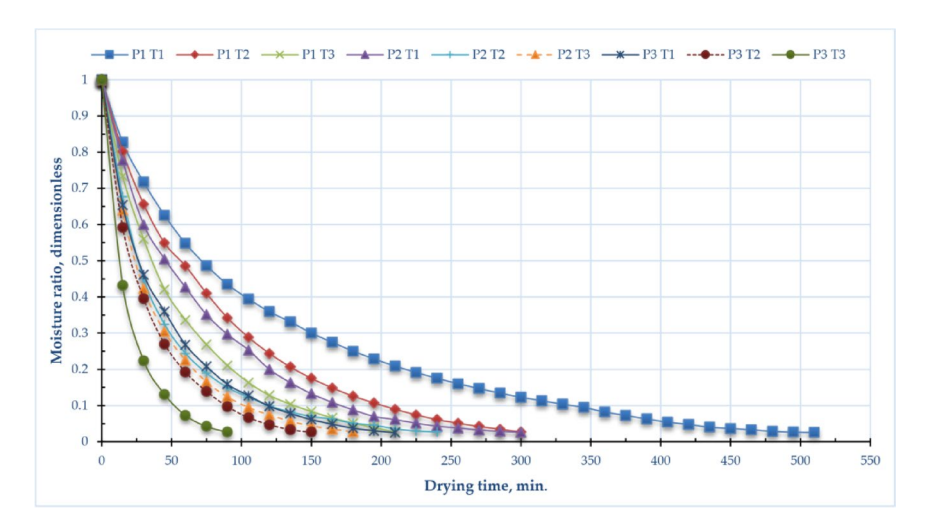


Fig. 4. Moisture ratio of sage leaves for DAVD at different levels of drying pressures (P1 = atm; P2 = -5 kPa and P3 = -10 kPa) and drying temperatures (T1 = 40, T2 = 50 and T3 = 60 °C).

	atm			−5 kPa			-10 kPa			
Coefficient	40 °C	50 °C	60 °C	40 °C	50 °C	60 °C	40 °C	50 °C	60 °C	
k	0.0069	0.0116	0.0164	0.0124	0.0143	0.0195	0.0171	0.0240	0.0398	
\mathbb{R}^2	0.9947	0.9987	0.9981	0.9959	0.9734	0.9915	0.9950	0.9964	0.9927	

Table 3. Drying constant (k) and coefficient determination (R^2) for experimental or observed of sage leaves for DAVD at different levels of drying pressures and drying temperatures.

Moisture ratio

Figure 4 illustrates the variation in operating pressure and drying temperatures concerning the moisture ratio of sage leaves. The drying duration necessary to achieve the equilibrium moisture content varied from 90 min to 510 min, contingent upon the operating pressure and drying temperature. Drying sage leaves under atmospheric pressure and 40 °C results in reaching the equilibrium moisture content after 510 min. The drying of sage leaves at an operating pressure of -10 kPa and a temperature of 60 °C resulted in the attainment of equilibrium moisture content after 90 min. The three exhibited a direct correlation between drying temperature and drying time and an inverse correlation between operating pressure and drying time. Reducing the working pressure from atmospheric pressure to -10 kPa decreases the drying time of the final product by about 142.9%, 100%, and 133.3% at drying temperatures of 40 °C, 50 °C, and 60 °C, respectively. This observation aligns with the findings of Beigi⁹⁸ and Kaleta et al.⁹⁶, which demonstrated that elevating the air temperature from 50 to 60 °C during drying enhanced mass transfer, shortened process duration, and decreased energy consumption. Where in vacuum drying, diminished pressure decreases the boiling point of water, facilitating moisture extraction at lower temperatures. This procedure reduces thermal degradation and energy usage. The moisture ratio, indicating the residual moisture content in relation to the initial quantity, diminishes more effectively under vacuum, rendering it a crucial element in enhancing drying kinetics and product quality^{24,99}.

Table 3 displays the drying coefficient (k) and determination coefficient (R^2) for sage leaves under different operating pressures and drying temperatures. The tabulated data indicated that as the drying air temperature in the DAVD increases, the drying coefficient (k) also rises. Furthermore, the drying coefficient exhibited a significant increase as the system pressure within the dryer was reduced. The value rose from 0.0069 to 0.0164 as the drying temperatures escalated from 40 to 60 °C under atmospheric pressure. Also, the value rose from 0.0124 to 0.0195 as the drying temperatures escalated from 40 to 60 °C at -5 kPa. Additionally, the value rose from 0.0171 to 0.0398 as the drying temperatures escalated from 40 to 60 °C, at -10 kPa. This aligns with prior research $^{53,95-97}$. No discernible trend can be observed in the coefficient of determination data. At atmospheric pressure, the minimum R^2 was recorded at 40 °C and the maximum at 50 °C, but at an operating pressure of $^{-10}$ kPa, the minimum value was noted at 60 °C and the maximum at 50 °C.

Drying rate

Figure 5 illustrates the drying rate of sage leaves at several drying pressures (P1 = atm; P2 = -5 kPa; P3 = -10 kPa) and temperatures (T1 = 40 °C; T2 = 50 °C; T3 = 60 °C). Figure 6 depicts the correlation between drying speeds and moisture content of sage leaves using DAVD at varying drying pressures and temperatures. At the onset of drying (t=0), the drying rate was zero. During the initial stage, the drying rate reached its maximum due to the rapid evaporation of free (unbound) moisture from the cellular structure. As the process progressed, the depletion of free water led to a gradual decline in the drying rate. This trend continued until the material reached

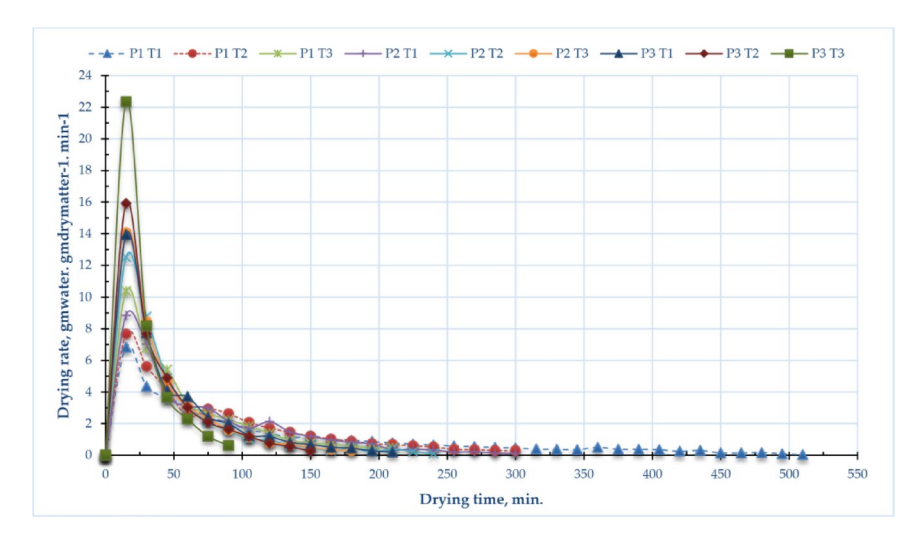


Fig. 5. Drying rate of sage leaves for DAVD at different levels of drying pressures (P1 = atm; P2 = -5 kPa and P3 = -10 kPa) and drying temperatures (T1 = 40, T2 = 50 and T3 = 60 °C).

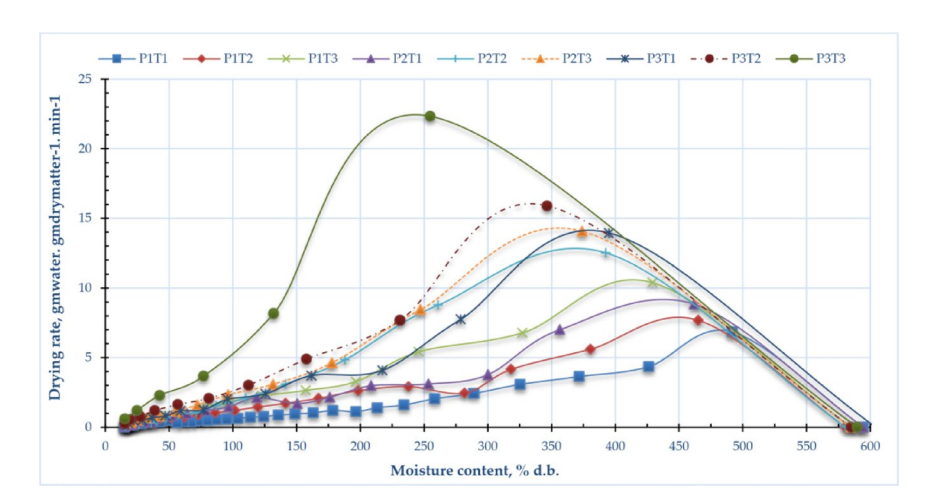


Fig. 6. Drying rate with moisture content of sage leaves for DAVD at different levels of drying pressures (P1 = atm; P2 = -5 kPa and P3 = -10 kPa) and drying temperatures (T1 = 40, T2 = 50 and T3 = 60 °C).

equilibrium moisture content, at which point drying effectively ceased. The elevated drying rates of sage leaf samples dried using DAVD varied from 6.85 to 10.39 kg water/kg dry matter/h, 8.84 to 14.07 kg water/kg dry matter/h, and 13.95 to 22.34 kg water/kg dry matter/h at drying temperatures of 40 to 60 °C, corresponding to operating pressures of atm, -5 kPa, and – 10 kPa, respectively. The data illustrated in Fig. 6 indicates a direct correlation between the drying rate and temperature, as well as between the drying rate and operating pressures, with the maximum drying rate recorded at a temperature of 60 °C and operating pressures of -10 kPa. The drying rate is substantially affected by both drying temperature and operating pressure. Increased drying temperatures expedite the process by supplying additional thermal energy, thereby facilitating moisture evaporation and internal diffusion. The operating pressure substantially influences the drying rate. Decreased pressures lower the boiling point of water, facilitating expedited evaporation at reduced temperatures, thereby enhancing drying efficiency.

Figure 7 illustrates the drying rate versus moisture content of sage leaves under different conditions of drying pressures (P1 = atmospheric pressure, P2 = -5 kPa, and P3 = -10 kPa) and temperatures (T1 = 40 °C, T2 = 50 °C, and T3 = 60 °C) in a DAVD (Drying Assisted by Vacuum Drying) system. The graph demonstrates how both reduced pressure and elevated temperature influence the drying kinetics, with lower pressures (P3) and higher temperatures (T3) likely accelerating moisture removal due to enhanced driving forces for evaporation. The trend suggests that the drying rate is highest at the initial stages when free moisture is abundant, then declines as moisture content decreases, eventually stabilizing near equilibrium. This behavior aligns with typical drying curves, where external conditions (pressure and temperature) significantly impact the rate of water removal.

The current study demonstrates that vacuum drying of sage leaves at 60 °C with reduced pressures (-10 kPa) achieves a significantly higher drying rate (22.34 kg_{water}/kg_{dry matter/h}) compared to conventional drying methods used for other herbs, as shown in Table 4. For instance, heat pump drying of amaranth leaves (5.0), oven drying

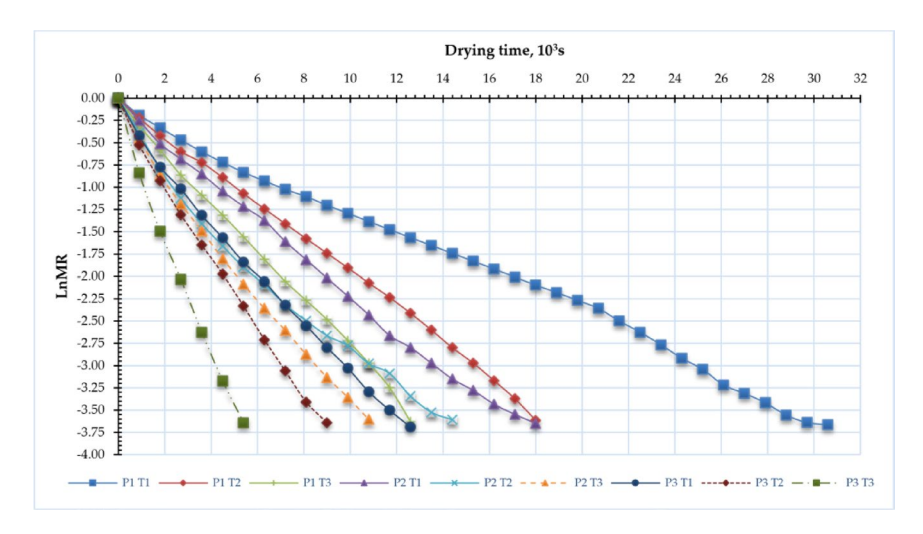


Fig. 7. Ln MR with drying time of sage leaves for DAVD at different levels of drying pressures (P1 = atm; P2 = -5 kPa and P3 = -10 kPa) and drying temperatures (T1 = 40, T2 = 50 and T3 = 60 °C).

Ref.	Product	Dryer type and drying conditions	Drying rate (kg _{water} / kg _{dry matter} /h)
100	Amaranth leaves	Heat pump dryer at drying temperature of 56 °C and air speed of 1.41 m/s.	5.0
101	Rue leaves	Oven electric dryer at drying temperature of 70 °C	3.55
24	Basil leaves	Hybrid solar dryer at drying temperature of 60 °C	1.7
102	Vernonia amygdalina leaves	Oven electric dryer at drying temperature of 60 °C	20
103	Coriander leaves	Microwave drying at 1000 W	6.0
103	Coriander leaves	Convective drying at drying temperature of 120 °C	2.3
Current study	Sage leaves	Vacuum dryer at drying temperature of 60 °C, and operating pressures of atm, $-5~\mathrm{kPa}$, and $-10~\mathrm{kPa}$	22.34

Table 4. Comparison between the achieved drying rate with previous studies.

of rue leaves (3.55), hybrid solar drying of basil (1.7), and even high-temperature convective drying of coriander (2.3) all yielded lower rates. While microwave and oven drying of Vernonia amygdalina leaves reached 20 and 6.0, respectively, the vacuum drying method in this study surpassed these values, highlighting its superior efficiency in moisture removal. This enhanced performance is attributed to the combined effect of elevated temperature and reduced pressure, which accelerates moisture diffusion while preserving product quality, making vacuum drying a promising technique for industrial-scale herb processing.

Effective moisture diffusivity (EMD)

Experimental data of moisture content has converged to construct portraits of ln (MR) over time (t) as depicted in Fig. 7. Where a linear connection between drying time and ln (MR) was discovered. The key experimental parameter typically employed for simulating drying processes is the reduction in sample mass, which is defined as the ratio between the water content at a specific time (t) and the original moisture content 104. The findings displayed in Fig. 8 demonstrate that the drying time is largely dictated by the internal mass transfer resistance, which is influenced by the existence of a decreasing rate drying phase. Consequently, the EMD values for the drying experiment under various situations are computed using Fick's second law. The EMD of the different sage samples was measured for different pressure settings and drying temperatures (Fig. 8). When the operating pressure reduced from atm to -100 kP, the EMD increased from 1.165×10^{-9} to 2.886×10^{-9} m²/s, from 1.959×10^{-9} to 4.053×10^{-9} m²/s, and from 2.774×10^{-9} to 6.716×10^{-9} m²/s, at drying temperatures of 40, 50, and 60 °C, respectively. On the other hand, when the drying temperatures increased from 40 °C to 60 °C, the EMD increased from 1.165×10^{-9} to 2.774×10^{-9} m²/s, from 2.094×10^{-9} to 3.283×10^{-9} m²/s, and from 2.886×10^{-9} to 6.716×10^{-9} m²/s, at operating pressures of atm, -5 kP, and -10 kP, respectively. This can be clarified as follows: An increase in air temperature and a reduction in operating pressure will accelerate the movement of water molecules, resulting in a heightened rate of water diffusion. This subsequently enhances the thermal and mass transfer between the solid-liquid film and the heated air. Consequently, the moisture concentration and partial pressure of water vapor on the leaf surface diminish, thereby expediting the internal evaporation, migration, and EMD processes within the sage leaves¹⁰⁵. Moreover, reducing pressure in a vacuum dryer markedly improves EMD by decreasing the boiling point of water, facilitating moisture evaporation at lower temperatures 106,107. This enhances the pushing power for moisture extraction and diminishes the barrier

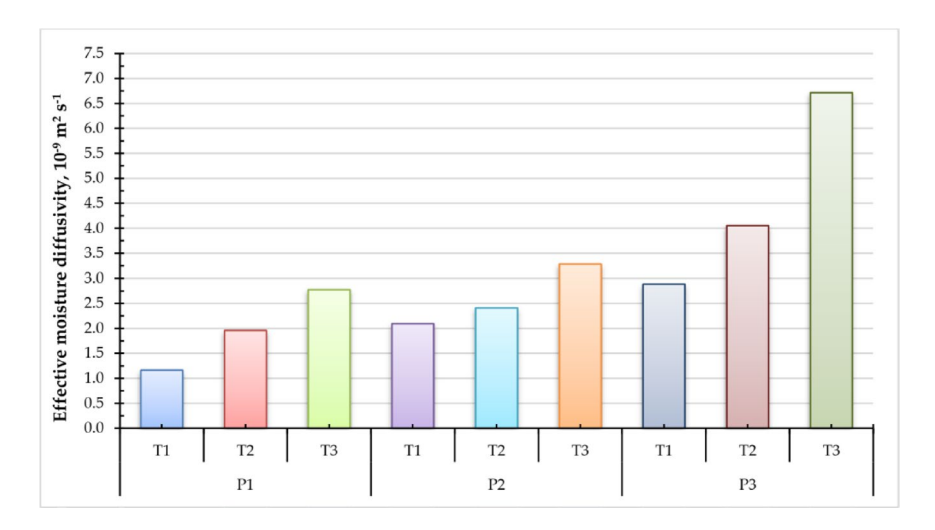


Fig. 8. Effective moisture diffusivity of sage leaves for DAVD at different levels of drying pressures (P1 = atm; P2 = -5 kPa and P3 = -10 kPa) and drying temperatures (T1 = 40, T2 = 50 and T3 = 60 °C).

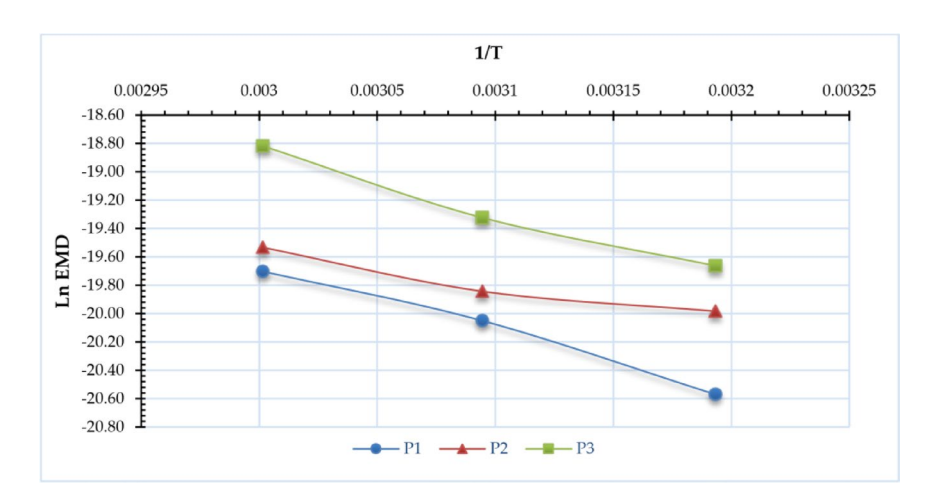


Fig. 9. LnEMD vs. 1/T of sage leaves for DAVD at different levels of drying pressures (P1 = atm; P2 = -5 kPa and P3 = -10 kPa).

to vapor diffusion within the material. The drying process becomes more efficient, especially for heat-sensitive substances, as enhanced diffusivity accelerates moisture transfer and improves overall drying kinetics. The EMD values acquired in the present study exceeded those reported in other research, including Ouahida's dried sage leaves, which utilized a convection oven at drying temperatures of 30, 45, and 60 °C, where the EMD varied from 1.1 to 3.7×10^{-12} m²/s m²/s. Additionally, Ahmed employed a microwave at three distinct power density levels of 6.7, 10, and 20 W/g for the desiccation of sage leaves, achieving a maximum EMD of 1.73×10^{-9} m²/s during the investigation. Doymaz and Karasu sessed the impact of air temperature on the EMD of sage leaves at temperatures of 45, 50, 55, 60, and 65 °C in a cabinet dryer, concluding that the EMD values were considerably influenced by temperature, ranging from 1.62×10^{-9} to 5.73×10^{-9} m²/s.

Activation energy

Figure 9 illustrates the correlation between ln (EMD) and (1/T). Also, Fig. 10 illustrates the activation energy of various sage leaf samples at distinct operating pressures, determined to determine the lowest energy required for drying to occur. Across the three tested operating pressures (P1 = atmospheric pressure, P2 = -5 kPa, P3 = -10 kPa), the activation energy exhibited a non-monotonic trend. Specifically, it decreased from 37.7 kJ/mol (P1) to 19.4 kJ/mol (P2) as the pressure was reduced from atmospheric to -5 kPa but then increased to 36.5 kJ/mol (P3) when the pressure was further lowered to -10 kPa. This suggests that the relationship between pressure and activation energy is not linear, possibly indicating competing mechanisms—such as enhanced moisture removal at moderate vacuum (-5 kPa) followed by altered mass transfer dynamics at higher vacuum levels (-10 kPa). The results are inferior to those reported by Ouahida⁶³, who dried sage leaves in a convection oven at three temperatures: 30, 45, and 60 °C, with an activation energy of 63.45 kJ/mol. And Doymaz and Karasu⁴⁵ assessed

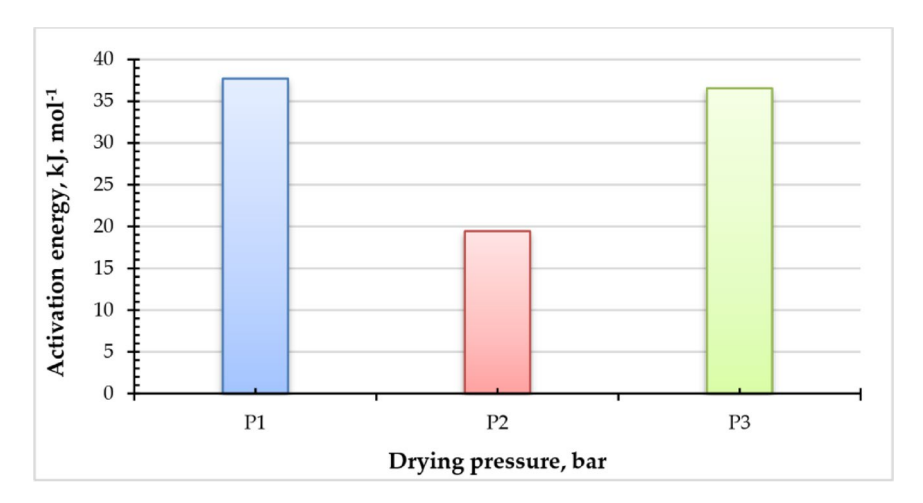


Fig. 10. Activation energy vs. drying of sage leaves at different levels of drying pressures (P1 = atm; P2 = -5 kPa and P3 = -10 kPa).

the impact of air temperature on the activation energy of sage leaves at 45, 50, 55, 60, and 65 °C in a cabinet dryer, concluding that the activation energy was 52.52 kJ/mol for these temperatures.

Mathematical modeling

The moisture content data collected during the drying experiment were transformed into the moisture ratio (MR) and fitted to the nine mathematical models presented in Table 5. Also, Table 5 presents the statistical outcomes of the various mathematical models, encompassing the drying model coefficients and the metrics employed to assess goodness of fit, specifically R^2 , R^2_{adj} , and RSME. Typically, R^2 and R^2_{adj} , values above 0.99, while RMSE values fell below 0.01. The R^2 and R^2_{adj} values of the Aghbashlo model were 0.81 and 0.78 at an operating pressure of -5 kPa for drying temperatures of 50 and 60 °C, respectively, and were 0.73 at an operating pressure of -10 kPa for a drying temperature of 40 °C. Figure 11 illustrates the comparison between the experimental moisture ratio at various drying temperatures and the predictions made by the Page model. The dots in Fig. 11 closely align along a 45-degree line, demonstrating a strong correlation between computed and experimental data, indicating that the Page model effectively characterizes the drying behavior of sage leaves. The Page model is deemed appropriate for characterizing the thin layer drying of sage leaves.

Thermodynamic properties of sage leaves

Equations 4 and 5 are applied to determine these parameters which are shown in Table 6. The values of ΔG^{\ddagger} corresponds to the average for the different drying temperatures. The results for all assays ($\Delta H^{\dagger} > 0$; $\Delta S^{\dagger} < 0$ and $\Delta G^{\ddagger} > 0$) indicate that the drying process of sage leaves is endothermic and not a spontaneous process^{109,110}. Activation enthalpy (ΔH‡) in the context of drying refers to the minimum energy required to initiate the process of moisture removal. This energy is needed to break the intermolecular bonds between water molecules and the material being dried, allowing water to transition from a liquid to a vapor phase. Higher activation enthalpy means more energy is needed to start the drying process, which can affect the efficiency and rate of drying 11,112 . Activation entropy (ΔS^{\ddagger}) describes the change in the degree of molecular disorder or randomness as the system transitions from the initial state (wet material) to the transition state (where water molecules are being released)^{113,114}Gibbs free energy of activation (ΔG^{\ddagger}) combines the effects of both activation enthalpy and activation entropy ($\Delta G^{\ddagger} = \Delta H^{\ddagger} - T\Delta S^{\ddagger}$) to provide a comprehensive measure of the energy barrier that must be overcome for drying to occur. It determines the overall spontaneity and rate of the drying process at a given temperature. A lower Gibbs free energy of activation means the drying process is more favorable and can proceed more readily, while a higher value indicates a greater energy barrier, making drying less efficient. Understanding these parameters helps in optimizing drying conditions for different materials 112,115,116. Activation enthalpy (\Delta H\frac{1}{2}) values (Table 6) decrease with increasing drying temperature and decreasing the operating pressure, as higher temperatures markedly increase the excitation of the product's water molecules compared to lower temperatures, hence diminishing the order of the water-product system 114,117,118. The activation entropy ($\Delta S \ddagger$), a thermodynamic parameter reflecting the molecular disorder during water-product interactions 113,114, exhibited temperature-independent behavior across the tested drying conditions. Contrary to typical expectations where entropy increases with temperature, ΔS‡ maintained consistent values despite variations in drying temperature. This remarkable invariance suggests the existence of a compensating mechanism in the system's free energy balance, where enthalpy and entropy changes offset each other to maintain thermodynamic stability throughout the drying process^{113,114}Negative entropy values are attributed to chemical adsorption and/or structural modifications of the adsorbent ^{118,119}. Gibbs free energy of activation (ΔG^{\ddagger}) (Table 6) indicates an endergonic reaction, requiring the infusion of energy into the air for the drying process of the product to occur. Comparable trends have been observed in investigations 112,115,116,118

				Models' con	stants value	es		Goodness	of fit indic	es
MMs	Pressure	T, °C	Parameters	Values	S.E.	p-value	Sign Insign.	RMSE	R ²	R ² adj.
			k ₁	0.01011	0.00028	2.76*10 ⁻²⁸	Sign.			
		40	k ₂	0.00134	0.00016	1.84*10-9	Sign.	0.017960	0.994832	0.994676
			k ₁	0.01297	0.00029	1.02*10 ⁻²⁰	Sign.			
	atm	50	k ₂	0.00065	0.00018	0.00168	Sign.	0.011982	0.998200	0.998105
			k ₁	0.01994	0.00033	2.77*10 ⁻¹⁷	Sign.			
		60	k ₂	0.00135	0.00020	1.34*10-5	Sign.	0.007374	0.999389	0.999342
			k ₁	0.01552	0.00040	1.54*10 ⁻¹⁹	Sign.			
		40	k ₂	0.00102	0.00024	0.00034	Sign.	0.013379	0.997707	0.997587
			k ₁	0.01062	0.00294	0.00254	Sign.			
Aghbashlo	-5kPa	50	k ₂	-0.00417	0.00210	0.06548	Insign.	0.118694	0.815249	0.802932
			k ₁	0.01029	0.00366	0.01688	Sign.			
		60	k ₂	-0.00556	0.00273	0.06636	Insign.	0.141263	0.780865	0.760944
			k ₁	0.02732	0.00077	2.43*10-14	Sign.			
		40	k ₂	0.00339	0.00043	2.86*10 ⁻⁶	Sign.	0.011646	0.998368	0.998242
			k ₁	0.01024	0.00452	0.04958	Sign.			
	-10kPa	50	k ₂	-0.00667	0.00346	0.08580	Insign.	0.165145	0.730648	0.700720
			k ₁	0.06047	0.00148	1.67*10 ⁻⁷	Sign.			
		60	k ₁	0.00650	0.00040	0.00052	Sign.	0.006348	0.999724	0.999669
			k	0.00827	0.00031	2.18E-23	Sign.			
	atm	40	a	0.90354	0.01369	8.97*10 ⁻³⁶	Sign.	0.021249	0.992986	0.992548
		10	С	0.03119	0.00818	0.00059	Sign.	0.021247	0.552500	0.552540
			k	0.03119	0.00032	1.61*10 ⁻¹⁸	Sign.			
		50	a	0.96336	0.00032	2.45*10 ⁻²⁶	_	0.012031	0.998281	0.998090
				0.90330	0.00943	0.23550	Sign.	0.012031		0.996090
			c k	0.00878	0.00713	7.60*10 ⁻¹⁴	Insign.			
		60		0.96278	0.00030	8.14*10 ⁻¹⁹	Sign.	0.010020	0.998762	0.000555
		60	a	0.90278	0.00979	0.00675	Sign.	0.010929		0.998555
			C L	0.02183		1.42*10 ⁻¹⁷	Sign.			
		40	k	0.95609	0.00043	1.42 10 1.12*10 ⁻²⁴	Sign.	0.014598	0.007414	0.997127
		40	a				Sign.	0.014598	0.997414	0.99/12/
			С	0.01477	0.00707	0.05118	Insign.			
T 11 1 (A (1)	51 D	50	k	0.02620	0.00079	1.09*10 ⁻¹⁴	Sign.	0.01.4250	0.005452	0.005111
Logarithmic (Asymptotic)	-5kPa	50	a	0.94357	0.01316	2.28*10 ⁻¹⁹	Sign.	0.014370	0.997473	0.997111
			C	0.04461	0.00547	1.10*10 ⁻⁶	Sign.			
			k	0.02838	0.00096	4.82*10 ⁻¹¹	Sign.			
		60	a	0.94914	0.01365	9.22*10 ⁻¹⁵	Sign.	0.014270	0.997967	0.997560
			С	0.03712	0.00719	0.00042	Sign.			
			k	0.02407	0.00108	3.98*10 ⁻¹¹	Sign.			
		40	a	0.93697	0.01795	1.61*10 ⁻¹⁵	Sign.	0.019617	0.995724	0.995012
			С	0.03576	0.00933	0.00238	Sign.			
			k	0.03159	0.00144	1.93*10 ⁻⁸	Sign.	1		
	-10kPa	50	a	0.95253	0.01765	1.54*10 ⁻¹¹	Sign.	0.017654	0.997264	0.996580
			С	0.03155	0.01025	0.01514	Sign.			
			k	0.05576	0.00276	3.53*10-5	Sign.			
		60	a	0.96192	0.01849	8.18*10 ⁻⁷	Sign.	0.016304	0.998545	0.997818
	1	1	c	0.03347	0.01111	0.03946	Sign.	1	1	

				Models' constants values				Goodness of fit indices		
MMs	Pressure	T, °C	Parameters	Values	S.E.	p-value	Sign Insign.	RMSE	R ²	R ² adj.
			k	0.02690	0.00126	4.28*10-20	Sign.			
			a	1.00617	0.00497	5.81*10 ⁻⁵⁰	Sign.			
		40	ь	-0.00006	0.00001	1.18*10-8	Sign.	0.005193	0.999594	0.999555
			n	0.75487	0.00939	1.52*10-37	Sign.			
		50	k	0.02014	0.00127	1.25*10-11	Sign.			
			a	0.99810	0.00554	2.44*10-29	Sign.			
	atm	50	ь	-7.74*10 ⁻⁵	1.82*10-5	0.00053	Sign.	0.005718	0.999633	0.999569
			n	0.88047	0.01409	1.58*10-21	Sign.			
			k	0.02817	0.00127	1.71*10-10	Sign.			
			a	1.00105	0.00403	5.58*10-22	Sign.			
		60	ь	-3.11*10 ⁻⁵	1.94*10-5	0.13685	Insign.	0.004076	0.999842	0.999799
			n	0.89168	0.01113	1.43*10-16	Sign.			
		k	0.02398	0.00221	4.48*10-9	Sign.				
		40	a	0.99816	0.00880	6.39*10 ⁻²⁶	Sign.			0.00000
			ь	-3.77*10 ⁻⁵	2.35*10-5	0.12687	Insign.	0.009033	0.999065	0.99890
			n	0.87618	0.02078	1.21*10-18	Sign.			
			k	0.04293	0.00428	1.75*10 ⁻⁷	Sign.			0.998406
	-5kPa	50	a	1.00463	0.01060	7.49*10 ⁻²⁰	Sign.			
Midilli			ь	0.00011	2.85*10 ⁻⁵	0.00184	Sign.	0.010677	0.998704	
			n	0.85296	0.02492	3.99*10-14	Sign.			
		60	k	0.04600	0.00261	2.79*10-8	Sign.		0.999731	0.999642
			a	1.00140	0.00545	2.12*10-17	Sign.			
			ь	5.41*10-5	2.67*10-5	0.07355	Insign.	0.005470		
			n	0.85422	0.01509	8.45*10 ⁻¹³	Sign.			
			k	0.04876	0.00196	5.00*10-11	Sign.			
			a	1.00025	0.00406	6.22*10 ⁻²²	Sign.			
		40	ь	-1.97*10 ⁻⁵	1.74*10-5	0.28183	Insign.	0.004085	0.999830	0.99978
			n	0.80409	0.01026	1.82*10 ⁻¹⁶	Sign.			
			k	0.05587	0.00144	2.00*10-9	Sign.			
			a	0.99998	0.00233	9.95*10 ⁻¹⁷	Sign.			
	-10kPa	50	ь	-4.62*10 ⁻⁵	1.69*10 ⁻⁵	0.0294	Sign.	0.002339	0.999958	0.99994
			n	0.82563	0.00724	1.05*10 ⁻¹²	Sign.			
			k	0.09224	0.00412	0.00020	Sign.			
			a	1.00004	0.00304	6.19*10 ⁻⁸	Sign.			
		60	b	-7.71*10 ⁻⁶	4.62*10 ⁻⁵	0.87813	Insign.	0.003040	0.999962	0.99992
			n	0.81636	0.01462	1.27*10-5	Sign.			

				Models' constants values				Goodness of fit indices			
MMs	Pressure	T, °C	Parameters	Values	S.E.	p-value	Sign Insign.	RMSE	R ²	R ² _{adj} .	
			k	0.02584	0.00088	1.17*10-24	Sign.				
		40	ь	-0.00006	0.00001	1.17*10-8	Sign.	0.005240	0.999574	0.999547	
			n	0.76197	0.00751	1.02*10-41	Sign.				
			k	0.02042	0.00096	3.06*10-14	Sign.				
	atm	50	ь	-7.89*10 ⁻⁵	1.72*10-5	0.00024	Sign.	0.005576	0.999631	0.999590	
			n	0.87773	0.01130	3.40*10-24	Sign.	1			
			k	0.02799	0.00101	3.14*10 ⁻¹²	Sign.				
	60	ь	-3.03*10-5	1.83*10-5	0.12456	Insign.	0.003915	0.999841	0.999815		
			n	0.89301	0.00950	1.41*10-18	Sign.				
			k	0.02427	0.00170	3.08*10 ⁻¹¹	Sign.				
		40	ь	-3.87*10-5	2.24*10-5	0.10193	Insign.	0.008790	0.999062	0.998958	
			n	0.87383	0.01702	5.66*10-21	Sign.]			
		50	k	0.04206	0.00359	1.29*10-8	Sign.		0.998685		
Modified midilli I	-5kPa		b	0.00011	2.75*10 ⁻⁵	0.00112	Sign.	0.010365		0.998497	
			n	0.85707	0.02235	1.40*10-15	Sign.				
			k	0.04571	0.00223	1.66*10-9	Sign.		0.999729	0.999675	
		60	b	5.47*10 ⁻⁵	2.53*10-5	0.05581	Insign.	0.005209			
			n	0.85556	0.01348	2.29*10-14	Sign.				
			k	0.04871	0.00165	1.43*10-12	Sign.				
		40	b	-1.96*10 ⁻⁵	1.66*10-5	0.26035	Insign.	0.003912	0.999830	0.999802	
			n	0.80434	0.00909	2.91*10 ⁻¹⁸	Sign.				
			k	0.05587	0.00124	6.68*10-11	Sign.				
	-10kPa	50	b	-4.62*10-5	1.58*10-5	0.01911	Sign.	0.002188	0.999958	0.999947	
			n	0.82563	0.00646	1.58*10 ⁻¹⁴	Sign.				
			k	0.09223	0.00349	1.22*10-5	Sign.				
		60	ь	-7.66*10 ⁻⁵	4.00*10 ⁻⁵	0.85742	Insign.	0.002633	0.999962	0.999943	
			n	0.81640	0.01253	3.32*10-7	Sign.]			

				Models' cor	istants value	es		Goodness	of fit indic	
MMs	Pressure	T, °C	Parameters	Values	S.E.	p-value	Sign. – Insign.	RMSE	R ²	R ² _{adj} .
			k	0.02671	0.00132	2.03*10-19	Sign.			
		40	a	1.04767	0.00973	1.81*10-41	Sign.	0.005570	0.000522	0.000407
		40	ь	-0.04120	0.00667	7.38*10 ⁻⁷	Sign.	0.005578	0.999532	0.999487
			n	0.74589	0.01125	5.74*10 ⁻³⁵	Sign.	1		
			k	0.02027	0.00121	5.01*10 ⁻¹²	Sign.			
	atm	50	a	1.03063	0.01035	5.79*10-22	Sign.	0.005.405	0.000661	0.000601
		50	b	-0.03196	0.00759	0.00059	Sign.	0.005497	0.999661	0.999601
			n	0.87062	0.01485	4.59*10-21	Sign.	1		
			k	0.02810	0.00129	2.15*10-10	Sign.			
		60	a	1.00863	0.00724	3.26*10 ⁻¹⁹	Sign.	0.004140	0.000026	0.000703
		60	ь	-0.00759	0.00530	0.17953	Insign.	0.004148	0.999836	0.999792
			n	0.89017	0.01260	5.70*10 ⁻¹⁶	Sign.	1		
			k	0.02437	0.00220	3.45*10-9	Sign.			
			a	1.01421	0.01358	7.60*10 ⁻²³	Sign.	1		
		40	ь	-0.01545	0.00877	0.09633	Insign.	0.008828	0.999107	0.998949
			n	0.86776	0.02238	4.95*10 ⁻¹⁸	Sign.	1		
			k	0.04050	0.00387	1.07*10 ⁻⁷	Sign.			
			a	0.97358	0.01138	2.84*10-19	Sign.	1		
Modified midilli I I	−5kPa	50	Ь	0.03022	0.00556	0.00011	Sign.	0.009450	0.998985	0.998751
			n	0.88081	0.02567	3.86*10 ⁻¹⁴	Sign.	1		
			k	0.04542	0.00256	2.62*10-8	Sign.			
			a	0.98892	0.00761	4.83*10 ⁻¹⁶	Sign.	-		
		60	ь	0.01231	0.00506	0.03775	Sign.	0.005223	0.999755	0.999673
			n	0.86246	0.01647	1.69*10 ⁻¹²	Sign.	1		
			k	0.04883	0.01047	5.60*10 ⁻¹¹	-			
						9.75*10 ⁻²⁰	Sign.	-		
		50	a	1.00542	0.00647		Sign.	0.004080	0.999830	0.999784
			b	-0.00513	0.00456	0.28461	Insign.	1		
			n 1-	0.80190	0.01164	7.46*10 ⁻¹⁶	Sign.			_
			k	0.05599	0.00142	1.78*10-9	Sign.	1	0.999960	
	-10kPa		a	1.00893	0.00412	5.00*10 ⁻¹⁵	Sign.	0.002290		0.999942
			Ь	-0.00890	0.00323	0.02822	Sign.	-		0,555512
			n	0.82169	0.00808	2.35*10 ⁻¹²	Sign.			
			k	0.09220	0.00427	0.00022	Sign.	-		
		60	a	1.00079	0.00624	5.35*10 ⁻⁷	Sign.	0.003044	0.999962	0.999924
			Ь	-0.00075	0.00535	0.89773	Insign.			
			n	0.81622	0.01724	2.08*10 ⁻⁵	Sign.			
		40	k	0.02139	0.00091	3.69*10-22	Sign.	0.008989	0.998706	0.998666
		<u> </u>	n	0.80779	0.00830	3.61*10 ⁻⁴²	Sign.			
	Atm	50	k	0.01750	0.00088	3.85*10 ⁻¹⁴	Sign.	0.008210	0.999155	0.999111
			n	0.91907	0.01079	5.20*10 ⁻²⁶	Sign.			
		60	k	0.02687	0.00077	2.95*10-14	Sign.	0.004177	0.999804	0.999789
			n	0.90502	0.00663	6.59*10 ⁻²²	Sign.	3.001177	3.555001	3.5557,05
		40	k	0.02241	0.00127	3.29*10 ⁻¹³	Sign.	0.009280	0.998897	0.998839
			n	0.89547	0.01245	1.30*10-24	Sign.	0.007200	0.770097	0.770039
Paga	-5kPa	50	k	0.05149	0.00466	1.31*10-8	Sign.	0.014270	0.997330	0.997152
Page	-3Kra	50	n	0.79730	0.02163	3.93*10-16	Sign.	0.014270	0.99/330	0.99/132
		60	k	0.04888	0.00205	8.17*10 ⁻¹¹	Sign.	0.005065	0.000000	0.000573
		60	n	0.83465	0.01043	1.45*10-16	Sign.	0.005967	0.999609	0.999573
		40	k	0.04743	0.00123	8.46*10 ⁻¹⁵	Sign.	0.0000==	0.000011	0.000=0-
		40	n	0.81237	0.00620	1.13*10-21	Sign.	0.003975	0.999810	0.999795
			k	0.05343	0.00121	7.56*10 ⁻¹²	Sign.			
	-10kPa	50	n	0.84013	0.00580	1.80*10 ⁻¹⁶	Sign.	0.002996	0.999911	0.999901
			k	0.09174	0.00216	1.36*10 ⁻⁷	Sign.			
		60	n	0.81831	0.00688	7.98*10 ⁻¹⁰	Sign.	0.002366	0.999962	2 0.999954
	_1				1	1000		1		

			Models' con	stants value	es .		Goodness	of fit indic	es
Pressure	T, °C	Parameters	Values	S.E.	p-value	Sign Insign.	RMSE	R ²	R ² _{adj} .
		b	-0.00528	0.00019	3.37*10-24	Sign.			
	40	a	7.05*10-6	4.84*10 ⁻⁷	6.24*10 ⁻¹⁶	Sign.	0.085043	0.884143	0.880632
		Ь	-0.00840	0.00029	4.64*10-17	Sign.			
Atm	50	a	1.81*10-5	1.24*10-6	8.41*10-12	Sign.	0.059109	0.956198	0.953893
		ь	-0.01228	0.00056	1.11*10-11	Sign.			
	60	a	3.83*10-5	3.31*10-6	3.20*10-8	Sign.	0.066352	0.950551	0.946747
	4.0	ь	-0.00910	0.00036	4.08*10-16	Sign.	0.054064		
	40	a	2.06*10-5	1.51*10-6	2.81*10-11	Sign.	0.071964	0.933662	0.930170
#1 P		ь	-0.01255	0.00078	7.37*10-11	Sign.	0.4400=4		
-5kPa	50	a	3.78*10 ⁻⁵	4.08*10 ⁻⁶	1.35*10 ⁻⁷	Sign.	0.1130/1	0.832339	0.821161
		ь	-0.01566	0.00097	5.43*10 ⁻⁹	Sign.			
	60	a	6.02*10-5	6.71*10 ⁻⁶	2.16*10-6	Sign.	0.092675	0.905685	0.897110
		ь	-0.01345	0.00080	3.09*10-10	Sign.	0.004500		
	40	a	4.44*10-5	4.73*10 ⁻⁶	3.65*10 ⁻⁷	Sign.	0.094699	0.892060	0.883757
101.0	50	ь	-0.01827	0.00120	1.02*10-7	Sign.	0.000042	0.022444	0.01.402
-10kPa	50	a	8.25*10-5	9.89*10-6	1.58*10-5	Sign.	0.088043	0.923444	0.914937
		ь	-0.03057	0.00275	0.00010	Sign.	0.006012	0.025000	0.022060
	00	a	0.00023	3.66*10-5	0.00156	Sign.	0.096813	0.935890	0.923068
	40	β	0.80779	0.00830	3.61*10 ⁻⁴²	Sign.			0.998666
		α	116.70	0.91973	5.87*10 ⁻⁴⁶	Sign.	0.008989	0.998706	
		β	0.91907	0.01079	5.20*10 ⁻²⁶	Sign.			
Atm	50	α	81.61	0.64681	3.03*10-29	Sign.	0.008210	0.999155	0.999111
		β	0.90502	0.00663	6.59*10-22	Sign.	0.004155	0.000004	0.000500
	60	α	54.40	0.27263	4.74*10-24	Sign.	0.0041//	0.999804	0.999789
	40	β	0.89547	0.01245	1.30*10-24	Sign.	0.000200	0.000005	0.000020
	40	α	69.53	0.68687	1.98*10-27	Sign.	0.009280	0.998897	0.998839
st-D.	50	β	0.79730	0.02163	3.93*10-16	Sign.	0.01.4270	0.007220	0.007152
-экра	50	α	41.29	0.89771	1.46*10-17	Sign.	0.0142/0	0.99/330	0.997152
	60	β	0.83465	0.01043	1.45*10-16	Sign.	0.005067	0.000,000	0.000572
	60	α	37.20	0.34647	5.72*10 ⁻¹⁸	Sign.	0.003967	0.999609	0.999573
	40	β	0.81237	0.00620	1.13*10-21	Sign.	0.003075	0.000010	0.999795
	40	α	42.64	0.25012	3.67*10-23	Sign.	0.0039/5	0.18666.0	0.999/93
10l-D	50	β	0.84013	0.00580	1.80*10-16	Sign.	0.002005	0.000011	0.000001
-10KPa	50	α	32.68	0.16395	1.02*10-17	Sign.	0.002996	0.999911	0.999901
	60	β	0.81831	0.00688	7.98*10 ⁻¹⁰	Sign.	0.002266	0.000062	0.000054
1	60	α	18.525	0.11210	1.54*10-10	Sign.	0.002366	0.999962	2 0.999954
	Atm -5kPa Atm -10kPa -10kPa	Atm 50 60 40 -5kPa 50 60 40 -10kPa 50 60 40 -5kPa 50 60 40 -5kPa 50 60 40 -40 -5kPa 50 60 40 -40 -40 -40	$Atm = \begin{vmatrix} 40 & b & & & \\ a & & & \\ 50 & b & & \\ a & & & \\ 60 & b & & \\ a & & & \\ 60 & b & & \\ a & & & \\ 60 & b & & \\ a & & & \\ 60 & b & & \\ a & & & \\ 60 & b & & \\ a & & & \\ 60 & b & & \\ a & & & \\ 60 & b & & \\ a & & & \\ 60 & b & & \\ a & & & \\ 60 & b & & \\ a & & & \\ 60 & b & & \\ a & & & \\ 60 & b & & \\ a & & & \\ 60 & & \\ 60 & & & \\ 60 & & & \\ 60 & & & \\ 60 & & & \\ 60 & & & \\ 60 & & \\ 60 & & & \\ 60 & & & \\ 60 & & & \\ 60 & & & \\ 60 & & & \\ 60 & & \\ 60 & & & \\ 60 & & & \\ 60 & & & \\ 60 & & & \\ 60 & & & \\ 60 & & \\ 60 & & & \\ 60 & & & \\ 60 & & & \\ 60 & & & \\ 60 & & & \\ 60 & & \\ 60 & & & \\ 60 & & & \\ 60 & & & \\ 60 & & & \\ 60 & & & \\ 60 & & \\ 60 & & & \\ 60 & & & \\ 60 & & & \\ 60 & & & \\ 60 & & & \\ 60 & & \\ 60 & & & \\ 60 & & & \\ 60 & & & \\ 60 & & & \\ 60 & & & \\ 60 & & \\ 60 & & & \\ 60 & & & \\ 60 & & & \\ 60 & & & \\ 60 & & & \\ 60 & & \\ 60 & & & \\ 60 & & & \\ 60 & & & \\ 60 & & & \\ 60 & & & \\ 60 & & \\ 60 & & & \\ 60 & & & \\ 60 & & & \\ 60 & & & \\ 60 & & \\ 60 & & & \\ 60 & & & \\ 60 & & & \\ 60 & & & \\ 60 & & & \\ 60 & & & \\ 60 & & \\$	$ \begin{array}{c ccccccccccccccccccccccccccccccccccc$	$ \begin{array}{c ccccccccccccccccccccccccccccccccccc$	$ \text{Atm} = \begin{cases} $	Pressure T, °C Parameters Values S.E. p-value Sign Insign. AH b -0.00528 0.00019 3.37*10-24 Sign. a 7.05*10-6 4.84*10-7 6.24*10-16 Sign. b -0.00840 0.00029 4.64*10-17 Sign. a 1.81*10-5 1.24*10-6 8.41*10-12 Sign. b -0.01228 0.00056 1.11*10-11 Sign. a 3.83*10-5 3.31*10-6 3.20*10-8 Sign. a 2.06*10-5 1.51*10-6 2.81*10-11 Sign. a 2.06*10-5 1.51*10-6 2.81*10-11 Sign. a 3.78*10-5 4.08*10-6 1.35*10-7 Sign. a 0.01255 0.00078 7.37*10-11 Sign. a 3.78*10-5 4.08*10-6 1.35*10-7 Sign. a 6.02*10-5 6.71*10-6 2.16*10-6 Sign. a 4.44*10-5 4.73*10-6 3.6*510-7 Si	$ \begin{array}{l l l l l l l l l l l l l l l l l l l $	$ \begin{array}{ c c c c c c c } \hline \textbf{Pressure} & \textbf{T, "C} \\ \hline \textbf{Pressure} & \textbf{Parameters} & \textbf{Values} & \textbf{S.E.} & \textbf{p-value} & \textbf{Sign.} & \textbf{Insign.} & \textbf{RMSE} & \textbf{R}^2 \\ \hline \textbf{Atm} & \textbf{b} & -0.00528 & 0.00019 & 3.37*10^{-24} & Sign. & 0.085043 & 0.884143 \\ \hline \textbf{Atm} & \textbf{50} & \textbf{b} & -0.00840 & 0.00029 & 4.64*10^{-17} & Sign. & 0.005109 & 0.956198 \\ \hline \textbf{a} & 1.81*10^{-5} & 1.24*10^{-6} & 8.41*10^{-12} & Sign. & 0.005109 & 0.956198 \\ \hline \textbf{a} & 3.83*10^{-5} & 3.31*10^{-6} & 3.20*10^{-8} & Sign. & 0.066352 & 0.95051 \\ \hline \textbf{a} & 3.83*10^{-5} & 3.31*10^{-6} & 2.81*10^{-11} & Sign. & 0.06100 & 0.00636 & 4.08*10^{-16} & Sign. & 0.071964 & 0.933662 \\ \hline \textbf{a} & 2.06*10^{-5} & 1.51*10^{-6} & 2.81*10^{-11} & Sign. & 0.071964 & 0.933662 \\ \hline \textbf{a} & 3.78*10^{-5} & 4.08*10^{-6} & 1.35*10^{-7} & Sign. & 0.113071 & 0.832339 \\ \hline \textbf{a} & 3.78*10^{-5} & 4.08*10^{-6} & 1.35*10^{-7} & Sign. & 0.113071 & 0.832339 \\ \hline \textbf{a} & 6.02*10^{-5} & 6.71*10^{-6} & 2.81*10^{-11} & Sign. & 0.092675 & 0.905685 \\ \hline \textbf{a} & 6.02*10^{-5} & 6.71*10^{-6} & 3.65*10^{-7} & Sign. & 0.092675 & 0.905685 \\ \hline \textbf{a} & 6.02*10^{-5} & 6.71*10^{-6} & 3.65*10^{-7} & Sign. & 0.094699 & 0.892060 \\ \hline \textbf{a} & 4.44*10^{-5} & 4.73*10^{-6} & 3.65*10^{-7} & Sign. & 0.094699 & 0.892060 \\ \hline \textbf{a} & 8.25*10^{-5} & 9.89*10^{-6} & 1.58*10^{-5} & Sign. & 0.094699 & 0.892060 \\ \hline \textbf{a} & 8.25*10^{-5} & 9.89*10^{-6} & 1.58*10^{-5} & Sign. & 0.098043 & 0.923444 \\ \hline \textbf{a} & 0.00023 & 3.66*10^{-5} & 0.00156 & Sign. & 0.008043 & 0.923444 \\ \hline \textbf{a} & 0.00023 & 3.66*10^{-5} & 0.00156 & Sign. & 0.008043 & 0.923444 \\ \hline \textbf{a} & 0.99907 & 0.00295 & 0.00656 & Sign. & 0.008989 & 0.998706 \\ \hline \textbf{a} & 0.80079 & 0.00380 & 3.61*10^{-42} & Sign. & 0.008910 & 0.998706 \\ \hline \textbf{a} & 0.91907 & 0.01079 & 5.20*10^{-26} & Sign. & 0.008210 & 0.999155 \\ \hline \textbf{a} & 0.91907 & 0.01029 & 5.20*10^{-26} & Sign. & 0.00417 & 0.99934 \\ \hline \textbf{a} & 0.9553 & 0.86867 & 1.98*10^{-27} & Sign. & 0.00417 & 0.999304 \\ \hline \textbf{a} & 0.9550 & 0.00650 & 0.00630 & 3.93*10^{-16} & Sign. & 0.00427 & 0.997330 \\ \hline \textbf{a} & 0.97930 & 0.02145 & 3.03*10^{-24} & Sign. & 0.004$

				Models' cor	nstants value	es		Goodness	of fit indic	es
MMs	Pressure	T, °C	Parameters	Values	S.E.	p-value	Sign Insign.	RMSE	R ²	R ² _{adj} .
		40	n	0.80779	0.00830	3.61*10-42	Sign.	0.008989	0.998706	0.998666
		40	δ	327.68	3.32442	2.39*10-42	Sign.	0.000909	0.998700	0.998000
	atm	50	n	0.91907	0.01079	5.20*10 ⁻²⁶	Sign.	0.008210	0.999155	0.999111
	aum		δ	202.24	2.1816	1.05*10-26	Sign.	0.008210	0.999133	0.999111
		<u></u>	n	0.90501	0.00663	6.59*10-22	Sign.	0.004177	0.999804	0.999789
		60	δ	136.73	0.91560	2.05*10-22	Sign.	0.004177	0.999804	0.539/89
		40	n	0.89547	0.01245	1.30*10-24	Sign.	0.009280	0.998897	0.998839
		40	δ	176.48	2.26408	2.81*10-25	Sign.	0.009280		
Weibullian I	−5kPa	50	n	0.79730	0.02163	3.93*10-16	Sign.	0.01.4270	0.997330	0.997152
weibuilian i	-5KPa		δ	117.52	3.01000	1.68*10-16	Sign.	0.014270		
			n	0.83465	0.01043	1.45*10-16	Sign.	0.005967	0.999609	0.999573
		60	δ	101.05	1.16095	5.74*10 ⁻¹⁷	Sign.	0.00596/	0.999609	0.9995/3
		40	n	0.81237	0.00620	1.13*10-21	Sign.	0.002075	0.999810	0.999795
		40	δ	119.03	0.85638	5.21*10-22	Sign.	0.003975	0.999810	0.999/95
	-10kPa	50	n	0.84013	0.00580	1.80*10-16	Sign.	0.002996	0.999911	0.999901
-1	-10KPa	30	δ	88.19	0.54987	7.24*10-17	Sign.	0.002996	0.999911	0.999901
		60	n	0.81831	0.00688	7.98*10 ⁻¹⁰	Sign.	0.002366	0.999962	0.000054
		60	δ	51.33	0.34393	2.56*10-10	Sign.	0.002366	0.999962	0.999954

Table 5. Mathematical models' constants values and goodness of fit indices results of Sage leaves at different levels of drying pressures and drying temperatures. *MMs* mathematical models, *T* drying temperature, ${}^{\circ}C$: k_1 , k_2 and k drying constants, min^{-1} ; a, b, c, n, α, β and δ: mathematical models constants or parameters, dimensionless, *S.E.* Standard error, *Sign.* – *Insign.* Significant – Insignificant at p ≤ 0.05, *RMSEE* The root mean square error, R^2 The coefficient of determination, R^2_{adj} . The adjusted coefficient of determination.

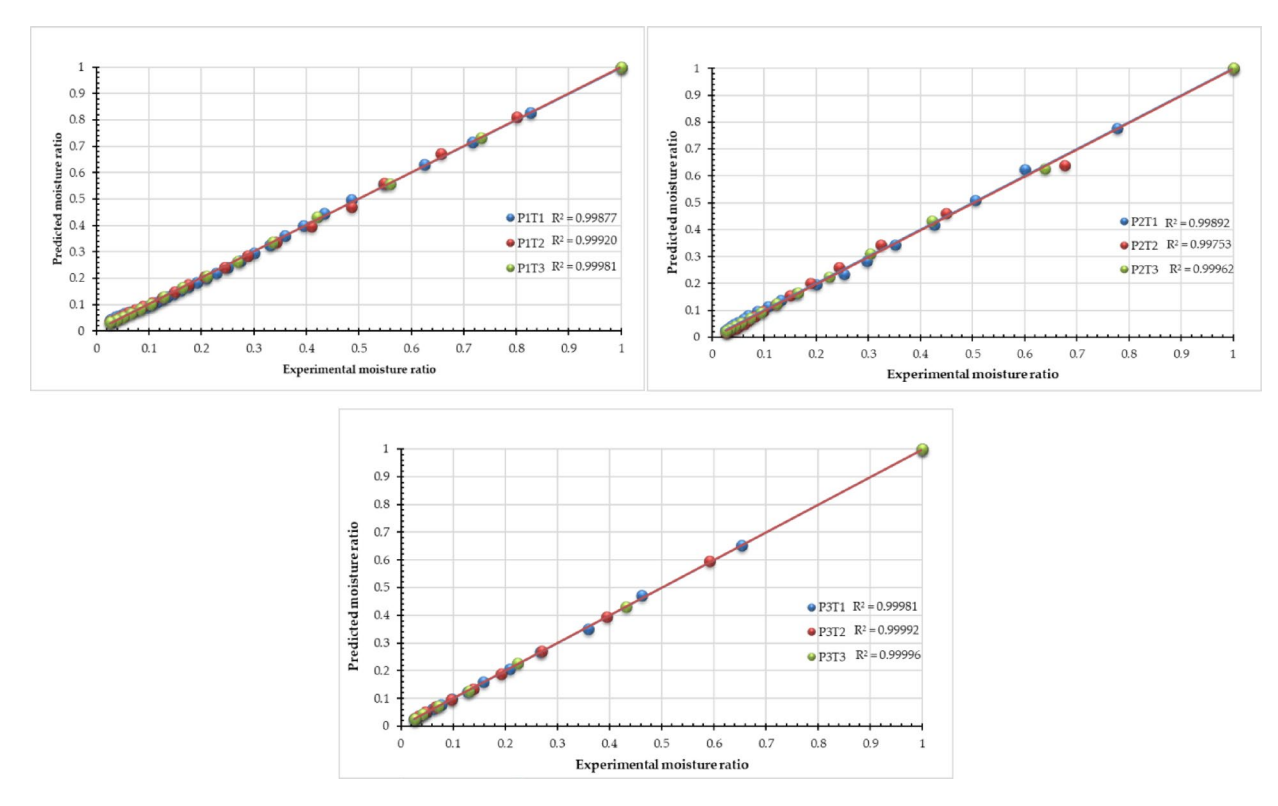


Fig. 11. Observed and predicted MR at different drying time for the best model (Page model) of sage leaves at different levels of drying pressures (P1 = atm; P2 = -5 kPa and P3 = -10 kPa) and drying temperatures (T1 = 40, T2 = 50 and T3 = 60 °C).

Temperature	Pressure	ΔH [‡] , kJ mol ⁻¹	ΔS [‡] , KJ mol ⁻¹ K ⁻¹	ΔG [‡] , kJ mol ⁻¹
	atm	35.10	-0.162	85.72
40 °C	−5 kPa	16.82	-0.108	50.54
	-10 kPa	33.95	-0.166	85.64
	atm	35.02	-0.162	87.27
50 °C	−5 kPa	16.73	-0.108	51.55
	-10 kPa	33.87	-0.165	87.22
	atm	34.93	-0.162	88.81
60 °C	−5 kPa	16.65	-0.108	52.56
	-10 kPa	33.78	-0.165	88.80

Table 6. Thermodynamic properties of Sage leaves for developing automatic vacuum drying system at drying pressures and drying temperatures.

Cost parameters	Unit
Capital cost, USD	300
Lifespan, years	20
Annual capital cost, USD	20.16
Annual maintenance cost, USD	0.61
Annual salvage value, USD	1.61
Annualized investment cost, USD	19.16

Table 7. Various costs related to the DAVD for drying Sage leaves.

	Drying temperature, °C & operating pressure, kPa								
	40 °C			50 °C			60 °C		
Economic analysis	atm	−5 kPa	-10 kPa	atm	−5 kPa	-10 kPa	atm	−5 kPa	-10 kPa
Specific energy consumption, KJ/kg	7344	5091.72	4095	5148	4728.4	3383.5	4006.8	3844.8	2160
Quantity of dried sage leaves, kg/year	823.6	1400	2000	1400	1750	2333.3	2000	2800	4666.7
Saving after 1 year	617.65	1050	1500	1050	1312.5	1750	1500	2100	3500
Payback period, year	0.509	0.301	0.211	0.301	0.241	0.181	0.211	0.151	0.091

Table 8. Economic parameters of the DAVD for drying Sage leaves.

Economic analysis

The performance analysis of DAVD is a quantitative assessment of economic processes that may aid policymakers, investors, and food processors in making educated decisions on crop drying systems. The study employed Eqs. 24–35, wherein the lifetime reduction strategy integrates the basic recovery process. The analysis considered critical variables, as evidenced by the data in Tables 7 and 8, while also accounting for the condition of the Libyan economy and the projected costs related to the DAVD components. Table 7 demonstrates that the capital cost of the DAVD is about 300 USD, significantly lower than alternative drying systems, with a life expectancy of 20 years. Table 7 indicates that the yearly capital and investment costs were 20.16 USD and 19.16 USD, respectively.

In Table 8, the bold numbers in colored boxes represented the lowest payback period at different drying temperatures and an operating pressure. It can be concluded that the lowest payback period was 0.091 year (about 1.11 months), achieved at a drying temperature of 60 $^{\circ}$ C and operating pressure of – 10 kPa, where the drying time is the lowest (90 min) and the annually dried qualities of sage leaves are the highest compared to other drying temperatures and operating pressures.

Conclusions, recommendations, and future work

In the present study, a Developed Automatic Vacuum Dryer (DAVD) was employed to investigate the drying kinetics of sage leaves under varying conditions. The experiments were conducted at three drying temperatures (40, 50, and 60 $^{\circ}$ C), three operating pressures (atmospheric pressure, – 5 kPa, and – 10 kPa), and a constant layer thickness of 1 cm. The key findings of this study are summarized as follows:

• Reducing the operating pressure from atmospheric pressure to -10 kPa significantly decreased the drying time, with reductions of 142.9%, 100%, and 133.3% at drying temperatures of 40 °C, 50 °C, and 60 °C, respectively.

- The maximum effective moisture diffusivity (EMD) of 6.716×10^{-9} m²/s was achieved under optimal drying conditions at 60 °C and -10 kPa, demonstrating the combined effect of elevated temperature and reduced pressure in significantly enhancing moisture migration.
- The minimum activation energy (19.4 kJ/mol) was achieved at an operating pressure of -10 kPa, indicating that higher vacuum levels significantly reduce the energy barrier for moisture diffusion.
- The drying behavior of sage leaves was analyzed using thin-layer drying models, with the Page model proving to be the most accurate in describing the drying characteristics. This model provided the best fit for the experimental data, confirming its suitability for predicting moisture loss in sage leaves under vacuum drying conditions.
- Thermodynamic parameters, including enthalpy (ΔH‡), entropy (ΔS‡), and Gibbs free energy (ΔG‡), were evaluated. The results (ΔH‡ > 0, ΔS‡ < 0, and ΔG‡ > 0) indicate that the drying process is endothermic (requiring energy input), Non-spontaneous (requires external conditions to proceed), and Entropically unfavorable (more ordered system during drying).
- An economic analysis of the DAVD revealed that drying sage leaves at 60 °C and 10 kPa not only optimized drying efficiency but also reduced the payback period to less than two months, demonstrating its cost-effectiveness for industrial applications.

Recommendations

The study highlights that vacuum drying at elevated temperatures (60 °C, -10 kPa) significantly improves drying efficiency while maintaining economic feasibility. The Page model effectively describes the drying kinetics, and thermodynamic analysis confirms the energy-intensive nature of the process. These insights can be valuable for scaling up sage leaf drying operations in the food and pharmaceutical industries, where preservation of bioactive compounds and energy efficiency are critical.

Future works

Future research should explore the effects of higher vacuum levels and varying layer thicknesses on drying efficiency and phytochemical retention in sage leaves. Advanced modeling (CFD, ANN) could optimize drying kinetics, while pilot-scale trials and hybrid drying systems (e.g., vacuum-microwave) should assess industrial scalability. Additionally, comparing vacuum drying with other methods (freeze-drying, convective drying) in terms of energy use and product quality is essential. Further studies could extend this approach to other herbs and heat-sensitive materials for broader applications.

Data availability

All data are provided within the article.

Received: 16 February 2025; Accepted: 20 May 2025

Published online: 29 May 2025

References

- Shukla, S. et al. Medicinal and aromatic plant cultivation, improvement and conservation for sustainable development. In Industrial Crops Improvement: Biotechnological Approaches for Sustainable Agricultural Development 183–204 (Springer, 2025).
- Valkovszki, N. J. et al. Influence of soil types on the morphology, yield, and essential oil composition of common Sage (Salvia officinalis L). Horticulturae 9, 1037 (2023).
- 3. Gali-Muhtasib, H., Hilan, C. & Khater, C. Traditional uses of Salvia Libanotica (East mediterranean sage) and the effects of its essential oils. *J. Ethnopharmacol.* 71, 513–520 (2000).
- 4. Lorenzo, J. M. et al. Understanding the potential benefits of thyme and its derived products for food industry and consumer health: from extraction of value-added compounds to the evaluation of bioaccessibility, bioavailability, anti-inflammatory, and antimicrobial activities. Crit. Rev. Food Sci. Nutr. 59, 2879–2895 (2019).
- 5. Arranz, E. et al. Supercritical Sage extracts as anti-inflammatory food ingredients. Ind. Crops Prod. 54, 159-166 (2014).
- Valdivieso-Ugarte, M., Gomez-Llorente, C., Plaza-Díaz, J. & Gil, Á. Antimicrobial, antioxidant, and Immunomodulatory properties of essential oils: A systematic review. Nutrients 11, 2786 (2019).
- Solomou, A. D. et al. Ecological value, cultivation and utilization of important medicinal plants (Sage, oregano and Sideritis) in Greece. Med. Plants Domest. Biotechnol. Reg. Import. 869–895 (2021).
- 8. Monder, M. J., Pacholczak, A. & Zajączkowska, M. Directions in ornamental herbaceous plant selection in the central European temperate zone in the time of climate change: benefits and threats. *Agriculture* 14, 2328 (2024).
- 9. Abdalrahman, Y. Assessing Land Degradation and Land Use in the Libyan Al-Jabal Alakhdar Region (Sheffield Hallam University (United Kingdom), 2013).
- 10. Laderach, P. et al. Strengthening climate security in the Middle East and North Africa Region. (IWMI, 2022).
- 11. Marotti, I. et al. Intercropping perennial fruit trees and annual field crops with aromatic and medicinal plants (MAPs) in the mediterranean basin. *Sustainability* 15, 12054 (2023).
- 12. Thamkaew, G., Sjöholm, I. & Galindo, F. G. A review of drying methods for improving the quality of dried herbs. *Crit. Rev. Food Sci. Nutr.* 61, 1763–1786 (2021).
- 13. Chua, L. Y. W., Chong, C. H., Chua, B. L. & Figiel, A. Influence of drying methods on the antibacterial, antioxidant and essential oil volatile composition of herbs: a review. *Food Bioproc Tech.* 12, 450–476 (2019).
- 14. Orphanides, A., Goulas, V. & Gekas, V. Drying technologies: vehicle to high-quality herbs. Food Eng. Rev. 8, 164–180 (2016).
- 15. Sethupathy, P. & Anandharamakrishnan, C. Challenges and opportunities. In *Conductive Hydro Drying of Foods* 445–471 (Elsevier, 2025).
- Oliveira, S. M., Brandao, T. R. S. & Silva, C. L. M. Influence of drying processes and pretreatments on nutritional and bioactive characteristics of dried vegetables: A review. Food Eng. Rev. 8, 134–163 (2016).
- 17. Chojnacka, K. et al. Improvements in drying technologies-Efficient solutions for cleaner production with higher energy efficiency and reduced emission. *J. Clean. Prod.* **320**, 128706 (2021).
- Jangam, S. V., Karthikeyan, M. & Mujumdar, A. S. A critical assessment of industrial coal drying technologies: role of energy, emissions, risk and sustainability. *Drying Technol.* 29, 395–407 (2011).

- 19. Ghanem, T. H. M. et al. Thin-layer modeling, drying parameters, and techno-enviro-economic analysis of a solar dried salted tilapia fish fillets. Sci. Rep. 15, 5073 (2025).
- 20. Eissa, A. S., Gameh, M. A., Mostafa, M. B. & Elwakeel, A. E. Some engineering factors affecting utilization of solar energy in drying tomato fruits introduction. 5, 52–68 (2024).
- 21. Elwakeel, A. E., Gameh, M. A., Eissa, A. S. & Mostafa, M. B. Recent advances in solar drying technology for tomato fruits: a comprehensive review. *Int. J. Appl. Energy Syst.* 6, 37–44 (2024).
- 22. Elwakeel, A. E. et al. Development and Techno-Economic analysis of a tracked indirect forced solar dryer integrated photovoltaic system for drying tomatoes. *Sustainability* 16, 7008 (2024).
- 23. Elwakeel, A. E. et al. Drying kinetics and thermo-environmental analysis of a PV-operated tracking indirect solar dryer for tomato slices. *PLoS One.* 19, e0306281 (2024).
- 24. Khater, E. S. G. et al. Assessment of a LPG hybrid solar dryer assisted with smart air circulation system for drying Basil leaves. *Sci. Rep.* 14, 23922 (2024).
- 25. Hill, D. S. Pests of Stored Foodstuffs and their Control (Springer Science & Business Media, 2002).
- Abdel-Khalek, H. H. Effect of gamma irradiation on the microbial, chemical quality and the biological activity of some spices and herbs. (2008).
- 27. Marcelino, S., Hamdane, S., Gaspar, P. D. & Paço, A. Sustainable agricultural practices for the production of medicinal and aromatic plants: evidence and recommendations. Sustainability 15, 14095 (2023).
- 28. Rahman, M. S. Handbook of Food Preservation (CRC Press, 2020).
- 29. Elghazali, M. N.; H. Z. T. Ř. A. G. and A. A. T. Effect Dehydration Methods Physicochemical Prop. Aswan Dry. Dates Introduction : 51, 50–64 (2020).
- 30. Scaman, C. H., Durance, T. D., Drummond, L. & Sun, D. W. Combined microwave vacuum drying. In *Emerging Technologies for Food Processing* 427–445 (Elsevier, 2014).
- 31. Li, X. et al. Chinese medicinal materials' drying technologies advancements-Principles, energy performance, and influence on the bioactive components. *Drying Technol.* 42, 1815–1845 (2024).
- 32. Radojčin, M. et al. Effect of selected drying methods and emerging drying intensification technologies on the quality of dried fruit: A review. *Processes* 9, 132 (2021).
- 33. Sangeeta, S. et al. Revolutionizing mushroom processing: innovative techniques and technologies. Food Chem. X 101774 (2024).
- Ghoshal, G. Emerging food processing technologies. In Food Processing for Increased Quality and Consumption 29–65 (Elsevier, 2018).
- 35. Lamidi, R. O., Jiang, L., Pathare, P. B., Wang, Y. & Roskilly, A. P. Recent advances in sustainable drying of agricultural produce: A review. Appl. Energy. 233, 367–385 (2019).
- 36. Acar, C., Dincer, I. & Mujumdar, A. A comprehensive review of recent advances in renewable-based drying technologies for a sustainable future. *Drying Technol.* 40, 1029–1050 (2022).
- 37. Venskutonis, P. R. Effect of drying on the volatile constituents of thyme (Thymus vulgaris L.) and Sage (Salvia officinalis L). Food Chem. 59, 219–227 (1997).
- 38. Sellami, I. H. et al. Drying Sage (Salvia officinalis L.) plants and its effects on content, chemical composition, and radical scavenging activity of the essential oil. *Food Bioproc Tech.* 5, 2978–2989 (2012).
- Sadowska, U., Kopeć, A., Kourimska, L., Zarubova, L. & Kloucek, P. The effect of drying methods on the concentration of compounds in Sage and thyme. J. Food Process. Preserv. 41, e13286 (2017).
- 40. Esturk, O. Intermittent and continuous microwave-convective air-drying characteristics of Sage (Salvia officinalis) leaves. *Food Bioproc Tech.* **5**, 1664–1673 (2012).
- Hamrouni-Sellami, I. et al. Total phenolics, flavonoids, and antioxidant activity of Sage (Salvia officinalis L.) plants as affected by different drying methods. Food Bioproc Tech. 6, 806–817 (2013).
- 42. Hassanain, A. A. Drying Sage (Salvia officinalis L.) in passive solar dryers. Res. Agricultural Eng. 57, 19 (2011).
- 43. Esturk, O., Arslan, M., Šoysal, Y., Uremis, I. & Ayhan, Z. Drying of Sage (Salvia officinalis L.) inflorescences by intermittent and continuous microwave-convective air combination. *Res. Crops.* 12, 607–615 (2011).
- 44. Belghit, A., Kouhila, M. & Boutaleb, B. Experimental study of drying kinetics of Sage in a drying tunnel working in forced convection. *J. Renew. Energies.* 2, 17–26 (1999).
- 45. Doymaz, İ. & Karasu, S. Effect of air temperature on drying kinetics, colour changes and total phenolic content of Sage leaves (Salvia officinalis). Qual. Assur. Saf. Crops Foods. 10, 269–276 (2018).
- 46. Salehi, F. & Kashaninejad, M. Effect of drying methods on rheological and textural properties, and color changes of wild Sage seed gum. *J. Food Sci. Technol.* **52**, 7361–7368 (2015).
- 47. Şahin-Nadeem, H., Dinçer, C., Torun, M., Topuz, A. & Özdemir, F. Influence of Inlet air temperature and carrier material on the production of instant soluble Sage (Salvia fruticosa Miller) by spray drying. *LWT-Food Sci. Technol.* **52**, 31–38 (2013).
- 48. Baltacı, C., Şidim, M. & Akşit, Z. Effects of spray and freeze-drying methods on aroma compounds, sensory characteristics, physicochemical composition, antioxidant and antimicrobial properties of instant Sage (Salvia Rosifolia Sm.) tea. *Turkish J. Anal. Chem.* 4, 19–30 (2022).
- 49. Amini, G., Salehi, F. & Rasouli, M. Effect of infrared drying on drying kinetics and color changes of wild sage seed mucilage.
- 50. Int, A. Official methods of analysis of AOAC Int. (2007).
- 51. Eke, A., Ben, Simonyan, K., J. DEVELOPMENT OF SMALL SCALE DIRECT & MODE PASSIVE SOLAR DRYERS FOR EFFECTIVE DRYING OF TOMATO. J. Appl. Agricultural Res. 6, 111–119 (2014).
- 52. El-Mesery, H. S. et al. Optimization of dried Garlic physicochemical properties using a self-organizing map and the development of an artificial intelligence prediction model. Sci. Rep. 15, 3105 (2025).
- 53. Metwally, K. A. et al. The mathematical modeling, diffusivity, energy, and Enviro-Economic analysis (MD3E) of an automatic solar dryer for drying date fruits. Sustainability 16, 3506 (2024).
- 54. ES, M., Hassan, M. A., Abdallah, Y. S. & Metwally, K. A. Effect of using a new automatic heating system powered by renewable energy on poultry houses. *Zagazig J. Agricultural Res.* **50**, 81–92 (2023).
- Etim, P. J., Eke, A. B. & Simonyan, K. J. Effect of air Inlet duct features and Grater thickness on cooking banana drying characteristics using active indirect mode solar dryer. Nigerian J. Technol. 38, 1056–1063 (2019).
- 56. Elwakeel, A. E. et al. Design and implementation of a PV-integrated solar dryer based on internet of things and date fruit quality monitoring and control. 2023 (2023).
- 57. Elmessery, W. M. et al. Deep regression analysis for enhanced thermal control in photovoltaic energy systems. Sci. Rep. 14, 30600 (2024).
- Rabha, D. K., Muthukumar, P. & Somayaji, C. Experimental investigation of thin layer drying kinetics of ghost Chilli pepper (Capsicum Chinense Jacq.) dried in a forced convection solar tunnel dryer. Renew. Energy. 105, 583–589 (2017).
- 59. Doymaz, İ. Drying characteristics and kinetics of Okra. J. Food Eng. 69, 275-279 (2005).
- 60. Temple, S. J. & Van Boxtel, A. J. B. Thin layer drying of black tea. J. Agric. Eng. Res. 74, 167-176 (1999).
- 61. Karathanos, V. T. & Belessiotis, V. G. Application of a thin-layer equation to drying data of fresh and semi-dried fruits. *J. Agric. Eng. Res.* 74, 355–361 (1999).
- 62. Doymaz, İ. & İsmail, O. Drying characteristics of sweet Cherry. Food Bioprod. Process. 89, 31–38 (2011).

- Ouahida, B. & Drying knetics desorption isotherms and apparent diffusivity of sage leaves. In *Defect and Diffusion Forum*. 406 173–181 (Trans Tech Publ, 2021).
- 64. Kara, C. & Doymaz, İ. Effective moisture diffusivity determination and mathematical modelling of drying curves of Apple pomace. *Heat Mass Transf.* 51, 983–989 (2015).
- 65. Crank, J. The Mathematics Ofdiffusion (Oxford University Press, 1975).
- 66. Osman, I. Drying characteristics of sweet Cherry. Food Bioprod. Process. 9, 31-38 (2010).
- 67. Coşkun, S., Doymaz, İ., Tunçkal, C. & Erdoğan, S. Investigation of drying kinetics of tomato slices dried by using a closed loop heat pump dryer. *Heat Mass Transf.* 53, 1863–1871 (2017).
- 68. Badaoui, O., Hanini, S., Djebli, A., Haddad, B. & Benhamou, A. Experimental and modelling study of tomato pomace waste drying in a new solar greenhouse: evaluation of new drying models. *Renew. Energy.* **133**, 144–155 (2019).
- 69. Samimi-Akhijahani, H. & Arabhosseini, A. Accelerating drying process of tomato slices in a PV-assisted solar dryer using a sun tracking system. *Renew. Energy.* **123**, 428–438 (2018).
- 70. Tagnamas, Z., Idlimam, A. & Lamharrar, A. Effect of microwave pretreatment on truffle solar drying from an energetic perspective. Food Front. 5, 994–1003 (2024).
- 71. Öksüz, H. B., Buzrul, S. & DrYFiT An excel freeware tool to describe thin layer drying of foods. *J. Food Process. Eng.* 47, e14748 (2024)
- 72. Midilli, A. & Kucuk, H. Mathematical modeling of thin layer drying of pistachio by using solar energy. *Energy Convers. Manag.* 44, 1111–1122 (2003).
- 73. Akpinar, E. K. & Bicer, Y. Mathematical modeling and experimental study on thin layer drying of strawberry. *Int. J. Food Eng.* 2, (2006)
- 74. Akpinar, E. K., Bicer, Y. & Cetinkaya, F. Modelling of thin layer drying of parsley leaves in a convective dryer and under open sun. *J. Food Eng.* **75**, 308–315 (2006).
- 75. Buzrul, S. Reassessment of thin-layer drying models for foods: a critical short communication. Processes 10, 118 (2022).
- 76. Inyang, U. E., Oboh, I. O. & Etuk, B. R. Kinetic models for drying techniques—food materials. Adv. Chem. Eng. Sci. 8, 27 (2018).
- 77. Henderson, S. M. Progress in developing the thin layer drying equation. Trans. ASAE. 17, 1167-1168 (1974).
- Inyang, U. E., Oboh, I. O. & Etuk, B. R. Kinetic models for drying techniques food materials. 27–48. https://doi.org/10.4236/aces.2018.82003 (2018).
- 79. Buzrul, S. Reassessment of thin-layer drying models for foods. Processes 10 (2022).
- 80. Ghazanfari, A., Emami, S., Tabil, L. G. & Panigrahi, S. Thin-layer drying of flax fiber: II. Modeling drying process using semitheoretical and empirical models. *Drying Technol.* 24, 1637–1642 (2006).
- 81. Ong, L. K. et al. Transesterification of leather tanning waste to biodiesel at supercritical condition: kinetics and thermodynamics studies. *J. Supercrit Fluids*. 75, 11–20 (2013).
- 82. Choi, C. S., Kim, J. W., Jeong, C. J., Kim, H. & Yoo, K. P. Transesterification kinetics of palm Olein oil using supercritical methanol. J. Supercrit Fluids. 58, 365–370 (2011).
- 83. Atheaya, D. Economics of solar drying. https://doi.org/10.1007/978-981-10-3833-4 (2017).
- 84. Prakash, O. & Kumar, A. Solar Drying Technology: Concept, Design, Testing, Modeling, Economics, and Environment (Springer, 2017).
- Kumar, M., Sahdev, R. K., Tiwari, S., Manchanda, H. & Kumar, A. Enviro-economical feasibility of groundnut drying under greenhouse and indoor forced convection hot air dryers. J. Stored Prod. Res. 93, 101848 (2021).
- 86. Elwakeel, A. E. et al. Advanced design and Engi-economical evaluation of an automatic sugarcane seed cutting machine based RGB color sensor. *PLoS One.* **19**, e0306584 (2024).
- Mohammed, I. A. & Al Dulaimi, M. A. K. An economic analysis of the costs of producing tomato under greenhouse in anbar governorate for the agricultural season 2019–2020. In *IOP Conference Series: Earth and Environmental Science* 904 12061 (IOP Publishing, 2021).
- 88. Singh, P. & Gaur, M. K. Environmental and economic analysis of novel hybrid active greenhouse solar dryer with evacuated tube solar collector. Sustain. Energy Technol. Assess. 47, 101428 (2021).
- 89. Wang, J. et al. Effects of various blanching methods on weight loss, enzymes inactivation, phytochemical contents, antioxidant capacity, ultrastructure and drying kinetics of red bell pepper (Capsicum annuum L). Lwt 77, 337–347 (2017).
- 90. Mukherjee, S. & Chattopadhyay, P. K. Whirling bed blanching of potato cubes and its effects on product quality. *J. Food Eng.* **78**, 52–60 (2007).
- 91. Kidmose, U. & Kaack, K. Changes in texture and nutritional quality of green asparagus spears (Asparagus officinalis L.) during microwave blanching and cryogenic freezing. *Acta Agriculturae Scand. Sect. B-Plant Soil. Sci.* 49, 110–116 (1999).
- 92. Etim, P. J., Eke, A., Ben & Simonyan, K. J. Design and development of an active indirect solar dryer for cooking banana. 8 (2020).
- 93. Tesfaye, A. & Habtu, N. G. Fabrication and performance evaluation of solar tunnel dryer for ginger drying. *Int. J. Photoenergy*. **2022**, 1–13 (2022).
- 94. Babar, O. A., Tarafdar, A., Malakar, S., Arora, V. K. & Nema, P. K. Design and performance evaluation of a passive flat plate collector solar dryer for agricultural products. *J. Food Process. Eng.* 1–13 (2020).
- Doymaz, İ. Evaluation of some thin-layer drying models of persimmon slices (Diospyros Kaki L). Energy Convers. Manag. 56, 199–205 (2012).
- 96. Kaleta, A., Górnicki, K., Winiczenko, R. & Chojnacka, A. Evaluation of drying models of Apple (var. Ligol) dried in a fluidized bed dryer. *Energy Convers. Manag.* 67, 179–185 (2013).
- 97. Meziane, S. Drying kinetics of Olive pomace in a fluidized bed dryer. Energy Convers. Manag. 52, 1644-1649 (2011).
- 98. Beigi, M. Hot air drying of Apple slices: dehydration characteristics and quality assessment. *Heat Mass Transf.* **52**, 1435–1442 (2016).
- Mansour, N. E., USING VACUUM DRYING SYSTEM FOR DRYING & SOME LEAFY MEDICINAL PLANTS. MISR J. AGRICULTURAL Eng. 40, 1–16 (2023).
- 100. Babu, A. K., Kumaresan, G., Raj, V. & Velraj, R. Experimental investigations of thin-layer drying of leaves in a heat-pump assisted tray-type batch drying chamber. *J. Mech. Eng. Stro. Vest.* **66**, (2020).
- 101. Mabasso, G. A. et al. Drying kinetics, thermodynamic properties and physicochemical characteristics of Rue leaves. *Sci. Rep.* 14, 14526 (2024).
- 102. Alara, O. R., Abdurahman, N. H. & Olalere, O. A. Mathematical modelling and morphological properties of thin layer oven drying of Vernonia amygdalina leaves. *J. Saudi Soc. Agricultural Sci.* **18**, 309–315 (2019).
- 103. Mouhoubi, K., Boulekbache-Makhlouf, L., Mehaba, W., Himed-Idir, H. & Madani, K. Convective and microwave drying of coriander leaves: kinetics characteristics and modeling, phenolic contents, antioxidant activity, and principal component analysis. *J. Food Process. Eng.* 45, e13932 (2022).
- 104. Bispo, J. A. C., Bonafe, C. F. S., Santana, K. M. O. V. & Santos, E. C. A. A comparison of drying kinetics based on the degree of hydration and moisture ratio. LWT-Food Sci. Technol. 60, 192–198 (2015).
- 105. Guan, Z., Wang, X., Li, M. & Jiang, X. Mathematical modeling on hot air drying of thin layer fresh tilapia fillets. *Pol. J. Food Nutr. Sci.* **63**, 25–34 (2013).
- 106. Parikh, D. M. Vacuum drying: basics and application. Chem. Eng. 122, 48-54 (2015).
- 107. Kerr, W. L. Food drying and evaporation processing operations. In *Handbook of Farm, Dairy and Food Machinery Engineering* 353–387 (Elsevier, 2019).

- Ahmed, T. H., DRYING SOME MEDICINAL & AND AROMATIC PLANTS BY MICROWAVE. Misr J. Agricultural Eng. 35, 953–974 (2018).
- 109. Spacino, K. R., Borsato, D., Buosi, G. M. & Chendynski, L. T. Determination of kinetic and thermodynamic parameters of the B100 biodiesel oxidation process in mixtures with natural antioxidants. *Fuel Process. Technol.* **137**, 366–370 (2015).
- 110. Gregório, A. P. H., Romagnoli, E. S., Borsato, D., Galvan, D. & Spacino, K. R. Kinetic and thermodynamic parameters in biodiesel oxidation reaction in the presence of coffee leaves and Sage extracts. *Sustain. Energy Technol. Assess.* 28, 60–64 (2018).
- 111. De Oliveira, G. H. H., Corrêa, P. C., Araujo, E. F., Valente, D. S. M. & Botelho, F. M. Desorption isotherms and thermodynamic properties of sweet corn cultivars (Zea mays L). *Int. J. Food Sci. Technol.* 45, 546–554 (2010).
- 112. Morais, M. F. et al. Modeling and thermodynamic properties of 'bacaba'pulp drying. *Revista Brasileira De Engenharia Agrícola E Ambiental.* **23**, 702–708 (2019).
- 113. de Goneli, A. L. D., Correa, P. C., de Oliveira, G. H. H. & Botelho, F. M. Water desorption and thermodynamic properties of Okra seeds. *Trans. ASABE.* 53, 191–197 (2010).
- 114. Ferreira Junior, W. N. et al. Modeling and thermodynamic properties of the drying of tamarind (Tamarindus indica L.) seeds. Revista Brasileira De Engenharia Agrícola E Ambiental. 25, 37–43 (2020).
- 115. Martins, E. A. S., Lage, E. Z., Goneli, A. L. D., Filho, H., Lopes, J. G. & C. P. & Drying kinetics of Serjania marginata Casar Leaves/ Cinetica de secagem de folhas de Timbo (Serjania marginata Casar). Revista Brasileira De Engenharia Agrícola E Ambiental. 19, 238–245 (2015).
- 116. Araujo, W. D., Goneli, A. L. D., Corrêa, P. C., Filho, H., Martins, E. A. S. & C. P. & Modelagem matemática Da secagem Dos Frutos de Amendoim Em Camada Delgada. *Revista Ciência Agronômica*. **48**, 448–457 (2017).
- 117. Corrêa, P. C., Oliveira, G. H. H., Botelho, F. M., Gonell, A. L. D. & Carvalho, F. M. Modelagem matemática e determinação Das propriedades termodinâmicas do café (Coffea Arabica L.) Durante O processo de secagem. *Revista Ceres.* 57, 595–601 (2010).
- 118. Kaveh, M., Zomorodi, S., Mariusz, S. & Dziwulska-Hunek, A. Determination of drying characteristics and physicochemical properties of mint (Mentha spicata L.) leaves dried in refractance window. *Foods* 13, 2867 (2024).
- 119. Moreira, R., Chenlo, F., Torres, M. D. & Vallejo, N. Thermodynamic analysis of experimental sorption isotherms of Loquat and quince fruits. *J. Food Eng.* **88**, 514–521 (2008).

Acknowledgements

The authors extend their appreciation to the Deanship of Scientific Research, King Saud University for funding through the Vice Deanship of Scientific Research Chairs; Research Chair of Prince Sultan Bin Abdulaziz International Prize for Water.

Author contributions

Conceptualization, N.E.M., K.A.M., and A.E.E., methodology, N.E.M., K.A.M., and A.E.E., software, N.E.M., K.A.M., and A.E.E., formal analysis, A.A.T., A.E., A.S., A.Z.D., A.M.O., and M.E.M., investigation, A.A.T., A.E., A.S., A.Z.D., A.M.O., and M.E.M., data curation, N.E.M., K.A.M., and A.E.E., writing-original draft, N.E.M., K.A.M., and A.E.E., writing - review and editing, N.E.M., K.A.M., and A.E.E., visualization, A.A.T., A.E., A.S., A.Z.D., A.M.O., and M.E.M., supervision, N.E.M., K.A.M., A.E.E., project administration, N.E.M., K.A.M., A.E.E., funding, A.S., A.Z.D., All authors have read and agreed to the published version of the manuscript.

Funding

Open access funding provided by University of Pécs.

This research was funded by the Deanship of Scientific Research, King Saud University through the Vice Deanship of Scientific Research Chairs; Research Chair of Prince Sultan Bin Abdulaziz International Prize for Water.

Declarations

Competing interests

The authors declare no competing interests.

Additional information

Correspondence and requests for materials should be addressed to K.A.M., A.S. or A.Z.D.

Reprints and permissions information is available at www.nature.com/reprints.

Publisher's note Springer Nature remains neutral with regard to jurisdictional claims in published maps and institutional affiliations.

Open Access This article is licensed under a Creative Commons Attribution 4.0 International License, which permits use, sharing, adaptation, distribution and reproduction in any medium or format, as long as you give appropriate credit to the original author(s) and the source, provide a link to the Creative Commons licence, and indicate if changes were made. The images or other third party material in this article are included in the article's Creative Commons licence, unless indicated otherwise in a credit line to the material. If material is not included in the article's Creative Commons licence and your intended use is not permitted by statutory regulation or exceeds the permitted use, you will need to obtain permission directly from the copyright holder. To view a copy of this licence, visit https://creativecommons.org/licenses/by/4.0/.

© The Author(s) 2025